Plant Cell Advance Publication. Published on June 4, 2018, doi:10.1105/tpc.18.00074

LARGE-SCALE BIOLOGY ARTICLE

Disrupted Genome Methylation in Response to High Temperature Has Distinct Affects on Microspore Abortion and Anther Indehiscence

Yizan Ma[a], Ling Min[a,*], Maojun Wang[a], Chaozhi Wang[a], Yunlong Zhao[a], Yaoyao Li[a], Qidi Fang[a], Yuanlong Wu[a], Sai Xie [a], Yuanhao Ding[a], Xiaojun Su [a], Qin Hu [a], Qinghua Zhang [a], Xueyuan Li [b], and Xianlong Zhang[a,*]

[a]National Key Laboratory of Crop Genetic Improvement, Huazhong Agricultural University, Wuhan 430070, Hubei, China
[b]Xinjiang Academy of Agricultural Science, Urumqi 830001, Xinjiang, China
[*]Corresponding Authors: xlzhang@mail.hzau.edu.cn and lingmin@mail.hzau.edu.cn

Short title: DNA methylation regulates male fertility

One-sentence summary: Integrated multi-omics data analysis reveals the role of genome methylation in male fertility, shedding light on the mechanism underlying male sterility in response to high temperature.

The authors responsible for distribution of materials integral to the findings presented in this article in accordance with the policy described in the Instructions for Authors (www.plantcell.org) are Xianlong Zhang (xlzhang@mail.hzau.edu.cn) and Ling Min (lingmin@mail.hzau.edu.cn)

ABSTRACT

High temperature (HT) stress induces male sterility, leading to yield reductions in crops. DNA methylation regulates a range of processes involved in plant development and stress responses, but its role in male sterility under HT remains unknown. Here, we investigated DNA methylation levels in cotton (*Gossypium hirsutum*) anthers under HT and normal temperature (NT) conditions by performing whole-genome bisulfite sequencing to investigate the regulatory roles of DNA methylation in male fertility under HT. Global disruption of DNA methylation, especially CHH methylation (where H=A, C or T), was detected in an HT-sensitive line. Changes in the levels of 24-nucleotide small-interfering RNAs were significantly associated with DNA methylation levels. Experimental suppression of DNA methylation led to pollen sterility in the HT-sensitive line under NT conditions but did not affect the normal dehiscence of anther walls. Further transcriptome analysis showed that the expression of genes in sugar and reactive oxygen species (ROS) metabolic pathways were

significantly modulated in anthers under HT, but auxin biosynthesis and signaling pathways were only slightly altered, indicating that HT disturbs sugar and ROS metabolism via disrupting DNA methylation, leading to microspore sterility. This study opens up a pathway for creating HT-tolerant cultivars using epigenetic techniques.

INTRODUCTION

DNA methylation represents an epigenetic mechanism for the regulation of gene expression (He et al., 2011; Zhang and Zhu, 2011; Jullien et al., 2012; Matzke and Mosher, 2014). DNA methylation of cytosines begins with the activation of DNA methyltransferases (DNMTs). The methylated cytosines are classified by sequence context as CG, CHG and CHH (H represents A, T or C) (Law and Jacobsen, 2010). Much research has shown that DNA methylation strongly influences many aspects of plant development, such as flower development, fruit ripening and stress responses (Kim et al., 2009; Zhong et al., 2013; Yong-Villalobos et al., 2015).

In *Arabidopsis thaliana*, DOMAINS REARRANGED METHYLTRANSFERASE2 (DRM2) catalyzes de novo DNA methylation in all contexts (Cao and Jacobsen, 2002). After the establishment of DNA methylation, METHYLTRANSFERASE1 (MET1) maintains methylation at CG sequences (Hu et al., 2014), CHROMOMETHYLASE3 (CMT3) maintains methylation at CHG (Cao and Jacobsen, 2002; Cao et al., 2003) and CMT2 maintains CHH methylation patterns (Shen et al., 2014). In plants, CG and CHG methylation patterns can be maintained by the recognition of hemimethylated signatures during DNA replication, but CHH methylation is not established by the same recognition process (Henderson and Jacobsen, 2007; Law and Jacobsen, 2010). An RNA-directed DNA methylation (RdDM) pathway guides *de novo* CHH methylation on strand-specific DNA sequences using a combination of 24-nucleotide small-interfering RNAs (24 nt siRNAs) (Matzke and Mosher, 2014). In the canonical RdDM pathway, specific transcripts are generated from plant-specific RNA polymerase (Pol IV) complexes. RNA-DEPENDENT RNA POLYMERASE2 (RDR2) then converts the transcripts into double stranded RNAs (dsRNAs). The 24 nt siRNAs are subsequently spliced by DICER-LIKE3 (DCL3). ARGONAUT4 (AGO4) binds to the 24 nt siRNAs to target

the silencing complex to the transcripts generated by Pol V. Finally, DRM2 interacts with AGO4 to target the CHH sites (Chan et al., 2004; Jia et al., 2009; Havecker et al., 2010; Matzke and Mosher, 2014).

When plants encounter stress, genome-wide transcriptional regulation occurs, including the activation of stress defense genes and regulatory proteins (Jiang et al., 2014; Le et al., 2014; Secco et al., 2015). Plants also require a mechanism to terminate these responses after stress. The transcriptional regulation of genes is closely linked with their epigenetic status (Iwasaki and Paszkowski, 2014). CHG and CHH DNA methylation usually participate in the regulation of heterochromatin formation and transcriptional gene silencing, while the methylation sites in gene bodies are predominantly in the CG context (Sijen et al., 2001; He et al., 2011; Melnyk et al., 2011).

There is increasing evidence that epigenetic regulation is essential for plant stress responses. In Arabidopsis, a large number of genes that respond to phosphate starvation are associated with hypo-methylation in their upstream regions (Yong-Villalobos et al., 2015). Mutants in the RdDM pathway show a lower survival rate compared to wild type under heat stress, indicating that the RdDM pathway is required for heat stress tolerance in plants (Popova et al., 2013).

Several studies have been carried out on the role of DNA methylation in male reproductive development. In Arabidopsis, DNA demethylation occurs in vegetative cells and sperm cells and is associated with the reactivation of transposable elements (TEs) and transposition. However, reactivated TEs do not initiate transposition in fertilized zygotes (Slotkin et al., 2009). siRNAs generated from retrotransposons accumulate in pollen and sperm cells, suggesting that epigenetic reprogramming occurs during reproductive development (Slotkin et al., 2009). Other studies have revealed that CG and CHG DNA methylation sites remain stable in the plant germline during development, but CHH methylation levels are reduced in retrotransposons of sperm cells and microspores. The lost CHH methylation is subsequently restored by RdDM in both fertilized embryos and vegetative cells (Calarco et al., 2012). These findings indicate that the epigenetic reprogramming, especially via RdDM in germ

cells, participates in the silencing of transposons and the regulation of development.

Previous DNA methylation studies have typically focused on model plants or seedlings under HT stress (Pecinka et al., 2010; Popova et al., 2013). Male reproductive organs are more sensitive to damage from environmental change than vegetative organs (Stromme et al., 2015). In a recent study, we detected changes in the levels of DNA methylation in cotton (*Gossypium hirsutum*) anthers under high temperature (HT) in both HT-tolerant and HT-sensitive cotton cultivars (Min et al., 2014). However, how DNA methylation is linked with male sterility under HT remains unclear. Here, we utilized the HT-tolerant cotton cultivar 84021 and HT-sensitive cotton cultivar H05 to uncover the role of DNA methylation during the HT response in anthers using whole genome bisulfite sequencing. Our results provide evidence for the mechanism by which HT disrupts DNA methylation to cause sterility in the anther, providing important insights into breeding using epigenetic techniques.

RESULTS

Single base resolution maps of DNA methylation in cotton anthers under high temperature (HT) stress

We previously identified two cotton lines that respond differentially to HT: 84021, which is HT-tolerant and H05, which is HT-sensitive. HT-induced male sterility in H05 is characterized by an indehiscent anther wall with abortive pollen grains, while 84021 shows normally developed anthers and pollen grains under HT (Figure 1A, B). High performance liquid chromatography (HPLC) analysis reveals different autologous genome methylation levels between 84021 and H05 under normal temperature (NT) conditions, and 84021 shows higher DNA methylation than H05 under HT (Min et al., 2014). To explore the roles of DNA methylation in male fertility under HT, we sampled anthers from 84021 and H05 at the tetrad stage (TS), tapetum degradation stage (TDS) and anther dehiscence stage (ADS) under NT and HT and performed whole-genome bisulfite sequencing (BS-seq).

After trimming adapters and filtering low-quality reads, approximately 1.2 billion paired-end reads were generated. There were more than 100 million cytosines covered

in each sample, a number sufficient for analysis (Supplemental Table 1). We used MethylKit (Akalin et al., 2012) software to evaluate the correlation between the replicates of each sample (Supplemental Figure 1). We used bisulfite-treated lambda DNA to evaluate the bisulfite conversion rate (Supplemental Table 2) and evaluated the false methylation rate by analyzing the methylation status of the mitochondrial genomes of each replicate per sample (Supplemental Table 3). The false methylation rates were relatively low compared to the results reported by Zhang et al., 2015a. We identified methylated cytosines using bismark_methylation_extractor software and binomial tests (Krueger and Andrews, 2011) (Supplemental Figure 2). Low methylated cytosines were all filtered out (Supplemental Figure 3), and ca. 63 to 93 million methylated-cytosines (mCs) in each sample were identified. Of these mCs, ca. 29 to 37 million mCs (~40% to 52% of total mCs) were in the CG context, ca. 23 to 30 million mCs (~32% to 41% of total mCs) were in the CHG context and ca. 4 to 25 million mCs (~6% to 27% of total mCs) were in the CHH context (Supplemental Figure 4, Supplemental Table 4). Among the three contexts, a large fraction of cytosines in the CG and CHG contexts were strongly methylated, while few CHH sites were methylated (Supplemental Figure 4). From the chromosome-scale viewpoint, CG and CHG methylation sites were enriched in heterochromatic regions, and CHH sites were relatively enriched in chromosomal arms compared to the pericentromere (Figure 1C, Supplemental Figure 5A-C). In the figure, the approximate centromere regions (Wang et al., 2015) are indicated by gray rectangles (Figure 1C) and light grey boxes (Supplemental Figure 5A-C). We constructed a website to show the profiles and details of DNA methylation of 84021 and H05 at the tetrad, tapetum degradation, and anther dehiscence stages under NT and HT (http://cgrd.hzau.edu.cn/cgi-bin/gb2/gbrowse/CottonReSequencing2016/).

The Hyper-CHH methylation on chromosomal arms may be driven by euchromatin-preferential transposable elements (TEs) in cotton anthers

DNA methylation usually occurs in heterochromatic regions, with the effect of preserving genome stability and silencing TEs. This has been confirmed in many species, including Arabidopsis, maize (*Zea mays*), rice (*Oryza sativa*) and cotton

(*Gossypium barbadense*) (Li et al., 2015; Zhang et al., 2015a; Rigal et al., 2016; Wang et al., 2016). However, in the present study, we found that CHH methylation sites were relatively enriched on chromosomal arms, i.e. in euchromatic regions.

Different CHH methylation patterns have been found in the different types of TEs (Song et al., 2013; Wang et al., 2016). To understand the basis of hyper-CHH methylation on chromosomal arms, we divided the TEs into short (<0.5 kb), medium (0.5–4 kb) and long (>4 kb) classes, as previously described (Wicker et al., 2007). We examined the distribution of these three types of TEs on the genome, finding that short and medium TEs represent a major proportion of TEs across the whole genome (Supplemental Data Set 1). There are more short TEs than medium and long TEs in every position of each chromosome, with long TEs distributed evenly on each chromosome in both the At and Dt subgenomes (Figure 1D).

We also analyzed the CHH methylation levels in the three types of TEs, including TE bodies and their upstream (-2 kilobase, -2kb) and downstream (+2 kilobase, +2kb) regions. No significant CHH methylation occurred in medium TE bodies, upstream or downstream regions. However, hyper-CHH methylation occurred in short and long TEs bodies, but not in their upstream or downstream regions (Figure 1E). These data demonstrate that short TEs are preferentially enriched on each chromosomal arm and that hyper-CHH methylation is initiated in the short TEs regions, which may lead to the hyper-CHH methylation observed on chromosomal arms.

HT-induced changes in CHH methylation patterns in 84021 and H05

To investigate the difference in DNA methylation patterns under HT, we examined the cytosines that were covered by sequencing reads in the two replicates of each sample and identified the methylated cytosines in both replicates for further analysis via binomial tests. We analyzed the changes in DNA methylation by comparing HT to NT treatments in the HT-tolerant 84021 and HT-sensitive H05 cultivars. No significant changes in the number of CG and CHG methylation sites were observed under HT conditions in 84021 or H05 at the three anther stages. However, significant changes in the number of methylation sites in the CHH context were observed (Figure 1F, Supplemental Figure 2, Supplemental Table 4). At the tetrad and tapetum

147 degradation stages, H05 had reduced CHH methylation under HT but increased CHH
148 methylation under HT at the anther dehiscence stage (Figure 1F). 84021 showed
149 increased CHH methylation under HT compared to NT conditions at the tetrad,
150 tapetum degradation, and anther dehiscence stages.

151 To decipher the patterns of variation in DNA methylation across the whole genome,
152 we divided the genome into 100 base pair (bp) regions with no overlaps to identify
153 differentially methylated regions (DMRs). All mCs were mapped to the
154 corresponding genome (At, Dt). Putative DMRs were pooled via Fisher's Exact test
155 (cutoff with p-value <0.05) (Calarco et al., 2012), followed by multiple testing
156 correction (FDR <0.05), and were subsequently classified into the CG, CHG and
157 CHH contexts (Supplemental Table 5, Supplemental Data Set 2-4). We then
158 calculated the ratio between the number of hyper-DMR and hypo-DMR sites in the
159 whole genome to investigate the relationship between DMRs and changes in whole
160 genome methylation in 84021 and H05. At the tetrad and tapetum degradation stages,
161 84021 presented a higher ratio of hyper-DMRs than H05 in the CG, CHG and CHH
162 contexts, indicating the existence of genome-wide hyper-methylation levels in 84021
163 under HT. At the anther dehiscence stage, both 84021 and H05 showed more
164 hyper-DMRs than hypo-DMRs under HT (Supplemental Table 5). To further explore
165 the function of DMRs, we analyzed the distribution of DMRs along the genome. We
166 mapped the DMRs to both the At and Dt subgenomes. DMRs in the CG and CHG
167 methylation contexts were randomly distributed (Supplemental Figure 6). However,
168 DMRs in the CHH context were distributed uniformly across the chromosomes
169 (Figure 2B), which contrasts with the data for soybean, wheat and cotton fibers (Song
170 et al., 2013; Gardiner et al., 2015; Wang et al., 2016). These results demonstrate that
171 changes in DNA methylation across the genome occur widely when anthers suffer HT
172 stress, with significant hyper-CHH methylation in HT-tolerant 84021 and hypo-CHH
173 methylation in HT-sensitive H05 at the tetrad and tapetum degradation stages under
174 HT.

175 **The RdDM pathway plays a central role in altering DNA methylation in cotton**
176 **anthers in response to HT**

Clear differences in CHH methylation were detected in 84021 and H05 anthers under HT, while CG and CHG showed only minor changes (Figure 1F). Given that RdDM can specifically initiate CHH methylation to regulate transcriptional gene silencing and contributes to chromatin remodeling during multiple stress responses, including responses to HT stress (Zhang and Zhu, 2011; Popova et al., 2013; Matzke and Mosher, 2014), we next focused on changes in the RdDM pathway in 84021 and H05 under HT conditions. First, we utilized the same samples used to perform BS-seq to perform small RNA sequencing in order to evaluate the effect of 24 nt siRNAs on DNA methylation (Supplemental Table 6). After adapter clipping and structural RNA filtering, the 24 nt siRNAs were mapped to the TM-1 cotton genome (Zhang et al., 2015b). We then selected uniquely mapped 24 nt siRNAs and analyzed their distribution on each chromosome. We found that the preferential enrichment of 24 nt siRNAs occurred on each chromosomal arm (Supplemental Figure 5D), which is similar to the distribution of hyper-CHH methylation sites. We carried out correlation analysis between CHH methylation levels, the number of 24 nt siRNAs, protein-coding genes, and TEs in each 1 mega-base (Mb) chromosomal region. We detected a high correlation (R=0.87) between CHH methylation levels and 24 nt siRNAs, as well as a high correlation (R=0.82) between the number of 24 nt siRNAs and protein-coding genes (Supplemental Figure 7). These results point to a possible relationship between CHH methylation and the density of 24 nt siRNAs.

To further confirm that 24 nt siRNAs actively contribute to altering CHH methylation under HT, we studies the effects of 24 nt siRNAs in the 1 Mb genomic regions. We partitioned the genome into 1 Mb bins: regions harboring 24 nt siRNAs (siRNA-mapped regions) were regarded as siRNA+ regions, and regions lacking siRNA-mapped regions were regarded as siRNA- regions. CHH methylation levels in siRNA+ and siRNA- regions were also identified (Figure 2A). At all three stages of anther development, all siRNA+ regions showed a higher hyper-methylation level than the siRNA- regions (Figure 2A). This result suggests that the genome-wide changes in CHH methylation under HT might be associated with 24 nt siRNAs. Therefore, we divided the genome into 100 bp regions to identify differentially

siRNA-mapped regions (DSRs), as previously reported (Gent et al., 2014), to identify changes in CHH methylation levels in DSRs. The density of siRNAs in each bin were normalized using the 10*Transcripts Per Kilobase Million (10*TPM) value for each sample. We compared HT to NT conditions and identified DSRs based on the criteria of 10*TPM of bins greater than 0 and changes of more than 2-fold. After identifying the DSRs, we mapped the hypo-DSRs and hyper-DSRs to 1 Mb genomic regions. The distribution of DSRs was similar to that of CHH DMRs (Figure 2B). We then calculated the CHH methylation levels of each DSR. The hyper-DSRs showed hyper-CHH methylation, while the hypo-DSRs showed hypo-CHH methylation (Figure 2C). Furthermore, we analyzed the expression of genes that participate in 24 nt siRNA generation and methylation initiation in the RdDM pathway, such as *RDR2*, *DCL3*, *HUA ENHANCER1* (*HEN1*), *AGO4* and *DRM2*. In H05, lower expression levels of these genes were detected at the tetrad and tapetum degradation stages under HT, while HT treatment increased the expression levels of these genes at the anther dehiscence stage. Meanwhile, these genes were all up-regulated in 84021 at the tetrad, tapetum degradation and anther dehiscence stages under HT. These results are consistent with the changes in CHH methylation levels detected in 84021 and H05 (Supplemental Figure 8). In conclusion, under HT, RdDM was disrupted in 84021 and H05 at the tetrad and tapetum degradation stages, which might be associated with reduced CHH methylation levels.

CHH methylation changes significantly in the promoter and downstream regions of protein-coding genes in anthers under HT conditions

Our results reveal whole genome-wide changes in CHH methylation under HT conditions and relatively high levels of CHH methylation on chromosomal arms. Given the consensus that chromosomal arms are enriched in protein-coding genes, an interaction between DNA methylation and the expression of protein-coding genes would be expected. To test this hypothesis, we first explored the genome-wide DNA methylation density of protein-coding genes. All of the identified mCs were mapped to genic regions, including gene body, promoter (-2kb) and downstream (+2kb) regions. Minor changes were detected in the CG and CHG contexts in protein-coding

gene regions in HT compared to NT conditions in anthers at the same stage (Supplemental Figure 9). However, CHH methylation levels were found to exhibit variation in the gene regions (Figure 3A), which is consistent with changes in the three methylation contexts (Figure 1F). We also found that CHH methylation mainly changed in the promoter and downstream regions, which is similar to the distribution of 24 nt siRNAs (Figure 3A and B). At the tetrad stage, 84021 showed lower CHH methylation levels than H05 under NT. However, 84021 showed little hyper-CHH methylation under HT, while H05 exhibited significantly reduced CHH methylation in the promoter and downstream regions under HT. At the tapetum degradation stage, compared to NT, there was little difference in CHH methylation in H05 under HT, but 84021 showed a small amount of hyper-CHH methylation under HT. Hyper-CHH methylation was found in both 84021 and H05 compared HT to NT at the anther dehiscence stage, while 84021 showed higher CHH methylation levels than H05 under HT (Figure 3A).

To visualize the relationship between DMR and protein-coding gene regions, we mapped DMRs in the CG, CHG and CHH contexts to promoter (-2kb), gene body and downstream (+2kb) regions. The results showed that more CG and CHG DMRs were mapped to gene bodies and that CHH DMRs mainly mapped to promoter and downstream regions (Supplemental Figure 10). Considering there were many more DMRs in the CHH context (Supplemental Table 5) and the higher enrichment of 24 nt siRNAs on the promoters (Figure 3B), we analyzed the effect of 24 nt siRNAs on the promoters of protein-coding genes. Genes with 24 nt siRNAs that were mapped to promoters were identified as P_siRNA+ genes, and other genes were classified as P_siRNA- genes. We then analyzed CHH methylation levels on the promoters of P_siRNA+ and P_siRNA- genes. At all stages of anther development and in both HT-tolerant and sensitive cotton under both HT and NT conditions, hyper-CHH methylation levels were higher on the promoter regions of P_siRNA+ genes compared to P_siRNA- genes (Figure 3C). Meanwhile, minor differences in CHH methylation levels were found between 84021 and H05 in anthers at the same stage, which further strengthens the conclusion that 24 nt siRNAs are responsible for

altering CHH methylation levels in gene promoter regions and regulating gene expression under HT conditions in anthers.

Different changes in the RdDM pathway were found between 84021 and H05 (Supplemental Figure 8). Therefore, to explore the specific interactions between 24 nt siRNAs and protein-coding genes in 84021 and H05, we analyzed P_siRNA+ genes. In anthers at the same developmental stage, P_siRNA+ genes detectable in all four samples (84021 under NT and HT conditions, H05 under NT and HT conditions) were identified as common genes, and the remaining genes were classified as 84021-specific or H05-specific P_siRNA+ genes (Figure 3D). At the tetrad and tapetum degradation stages, there was little difference in the number of specific P_siRNA+ genes in 84021 vs. H05 under NT conditions, but H05 had fewer specific P_siRNA+ genes than 84021 under HT, suggesting weaker RdDM regulation at these stages in H05 under HT (Figure 3D). At the anther dehiscence stage, both 84021 and H05 had more specific P_siRNA+ genes, indicating that RdDM was strengthened in these two samples under HT. We subjected the sample-specific P_siRNA+ genes to gene ontology (GO) analysis to identify any enriched pathways. Oxidoreductase activity and carbohydrate binding were found to be enriched (Figure 3D), suggesting that genes involved in energy metabolism and redox homeostasis might be regulated by RdDM under HT.

Global depression of DNA methylation leads to pollen sterility

The HT-sensitive line H05 showed reduced DNA methylation levels under HT conditions. We hypothesized that reduced DNA methylation has a negative effect on male fertility under HT. To further investigate the role of DNA methylation in male sterility caused by HT stress, we treated H05 plants with Zebularine (Zeb), a DNA methylation inhibitor. We applied four different treatments via spray application to buds: 150 μM Zeb solution to H05 under NT and HT conditions [HNZ (H05+NT+Zeb), HHZ (H05+HT+Zeb)], and water under NT and HT to H05 as controls [HNW (H05+NT+Water), HHW (H05+HT+Water)]. After treatment, we carried out tissue sectioning of treated anthers to determine any developmental effects of the treatments.

Under control treatments, both HNW and HHW showed normal tetrad formation (Figure 4A, B) and normal callose staining with aniline blue (Figure 4 A', B') at the tetrad stage. No significant difference in tetrad or tapetum formation was found at the tetrad stage (Figure 4A, B). At the tapetum degradation stage, normally formed microspores were observed in HNW-treated anthers (Figure 4C), but HHW treatment led to the production of shriveled microspores with fewer inclusions (Figure 4D); this microspores phenotype is similar to a previously reported male sterility phenotype (Cecchetti et al., 2008; Cecchetti et al., 2017). At the anther dehiscence stage, pollen was released normally from HNW anthers (Figure 4E), while plants treated with HHW had completely shriveled pollen grains and an indehiscent anther wall (Figure 4F). These results further confirmed the distinct male reproductive phenotype of H05 under NT and HT conditions.

In response to Zeb treatment, both HNZ and HHZ showed normal tetrad formation at the tetrad stage (Figure 4a, b). Abnormal microspores were detected under both NT and HT in response to Zeb treatment at the tapetum degradation stage (Figure 4c, d). At the anther dehiscence stage, HHZ showed indehiscent anther walls and abnormal pollen grains (Figure 4f), which was similar to the phenotype observed under HHW treatment (Figure 4F). Unexpectedly, the anther endothecium of HNZ dehisced normally but contained barren pollen grains (Figure 4e).

Anther dehiscence is related to the thickness of secondary walls of the endothecium (Mitsuda et al., 2005; Zhao et al., 2010). We therefore performed aniline blue staining of anther tissue sections to examine secondary wall thickening in the endothecium. At the tetrad stage, no significant changes in tetrads were found in any of the treatment groups (Figure 4A', B' and a', b'). At the tapetum degradation stage, only the HNW (H05+NT+Water) treatment group had normally shaped microspores (Figure 4C', D' and c', d'). At the anther dehiscence stage, secondary wall thickening in the endothecium was observed under HT (Figure 4F', f'). There was little difference in secondary wall thickening following Zeb treatment compared to the controls (Figure 4E', e' and F', f'). Therefore, HT induced severe microspore sterility and secondary wall thickening of the endothecium in H05, but the suppression of DNA methylation

disrupted microspore development, with minor effects on secondary wall thickening in the endothecium. These results suggest that HT stress disrupts DNA methylation, which affects microspore development and has minor effects on anther dehiscence.

Suppression of DNA methylation disrupts gene and TE transcription in anthers

Disordered DNA methylation lead to abnormal development due to disrupted gene and TE expression (Hu et al., 2014; Zhang et al., 2015a). We hypothesized that the observed shrunken pollen grain observed in response to Zeb treatment might be due to disordered DNA methylation. First, we performed BS-seq on anthers at the tapetum degradation stage treated with HNZ and HHZ to evaluate the changes in DNA methylation under Zeb treatment (Supplemental Table 7). Reduced DNA methylation levels under Zeb treatment were observed based on the BS-seq data (Supplemental Figure 11). To further test this hypothesis, we subjected Zeb-treated and control samples to RNA-sequencing to identify transcriptional changes (Supplemental Table 8). We detected an increasing number of differentially expressed TEs in H05 under HT treatment, while Zeb treatment led to increased numbers of differentially expressed TEs under both NT and HT conditions (Supplemental Table 9). We also examined changes in gene expression in H05 following Zeb application and identified differentially expressed genes (DEGs) using Tophat2 and Cuffdiff software. There were more DEGs in H05 following Zeb treatment under both NT and HT treatment compared to the controls (Supplemental Figure 12, Supplemental Table 10). Given the previous finding that the unexpected transcription of TEs could results in severe growth defects in plants (Hu et al., 2014; Zhang et al., 2015a), we propose that HT disrupts whole-genome methylation, removes DNA methylation on TEs and genes, and leads to their unregulated transcription in H05. Zeb treatment might mimic the HT-induced disruption of hypo-methylation and induce unexpected transcription of TEs and genes in H05.

Changes in the sugar metabolism pathway under HT and following suppression of DNA methylation

To understand how changes in DNA methylation under HT stress disrupt gene expression and lead to pollen abortion, we identified DEGs under control (water) vs.

Zeb treatment and subjected them to Gene Ontology (GO) enrichment analysis. Under HT treatment, the DEGs from H05 sprayed with water were enriched in the GO categories 'carbohydrate metabolic process', 'plant hormone response', and especially 'auxin signaling' (ARF signaling) and 'oxidoreductase activity' (Supplemental Figure 13), which suggests that energy metabolism, auxin signaling and redox homeostasis are altered by HT stress in anthers. Among DEGs under Zeb treatment, we found that the GO categories 'carbohydrate metabolic process' and 'response to oxidative stress' were further enriched, but no significant enrichment observed in the category 'plant hormone response' (Supplemental Figure 13). These results suggest that greater energy consumption and changes in redox status occur in H05 under Zeb treatment than under HT stress.

To further investigate any changes in carbohydrate content under Zeb or HT treatment, we carried out total soluble sugar and starch assays. At the tetrad and tapetum degradation stages, both HT and Zeb treatment induced the accumulation of soluble sugars, with combined HT and Zeb treatment affecting the soluble sugar content more strongly than single treatments (Figure 5A). At the anther dehiscence stage, significant accumulation of soluble sugar was detected following Zeb treatment under both NT and HT conditions compared to the respective controls (Figure 5A). Starch content showed an opposite trend to soluble sugar content in all samples (Figure 5B). We also found that DNA methylation levels on the promoters of several amylase genes were negatively correlated with the expression levels at the three developmental stages, suggesting that amylase genes are regulated by DNA methylation (Figure 5C). The results of starch (I_2-KI) staining of pollen grains following HNW (H05+NT+Water), HNZ (H05+NT+Zeb), HHW (H05+HT+Water) and HHZ (H05+HT+Zeb) treatment strengthened our conclusion that HT induces DNA methylation that disrupts carbohydrate metabolism in pollen (Figure 5D). We therefore conclude that HT alters the DNA methylation status, leading to the excessive expression of amylase genes, thereby resulting in starch hydrolysis and a higher sugar concentration.

HT-induced DNA methylation is associated with ROS generation but not with

auxin accumulation in anthers

The GO term ‘oxidoreductase activity’ was further enriched following the DNA suppression assay, as described above. We then performed a hydrogen peroxide (H_2O_2) assay to investigate the redox status of pollen under HT or Zeb treatment. At the tetrad stage, HT or Zeb treatment induced a higher level of H_2O_2 in HT-sensitive H05 (Figure 6A). At both the tapetum degradation and anther dehiscence stages, H05 generated more H_2O_2 when under HT coupled with Zeb, similar to the results for soluble sugar (Figure 6A). Since it is generally considered that H_2O_2 is synthesized by respiratory burst oxidase homolog (RBOH) proteins (Mittler et al., 2004; Marino et al., 2012), we analyzed the expression and DNA methylation levels of all *RBOH* genes . Several *RBOH* genes were up-regulated under HT, which was associated with hypo-methylation of promoter regions (Figure 6B), as well as H_2O_2 concentrations (Figure 6A).

To further investigate ROS generation in pollen, we performed a ROS staining assay on the same four treatment groups used for starch staining [HNW (H05+NT+Water), HNZ (H05+NT+Zeb), HHW (H05+HT+Water) and HHZ (H05+HT+Zeb)]. The results show that Zeb or HT significantly induces ROS generation in H05 (Figure 6C), and HT combined with Zeb induced additional ROS generation in H05. We therefore speculate that HT induces hypo-methylation to release the *RBOH* genes from silencing, thereby leading to the enhanced generation of H_2O_2 under HT.

Auxin contributes to the control of anther dehiscence by regulating endothecium lignification and the jasmonic acid pathway in Arabidopsis (Cecchetti et al., 2013). We previously showed that HT alters auxin metabolism and signaling and causes anther abortion in cotton (Min et al., 2014). The DEGs under HT treatment show significant enrichment for the GO term 'hormone response pathway', but the DEGs under Zeb treatment did not. Therefore, we investigated whether the changes in auxin metabolism and signaling pathways might be caused by disrupted DNA methylation under HT.

We investigated the expression of auxin biosynthesis genes at the anther dehiscence stage and found that several auxin biosynthesis genes (such as *ALDEHYDE*

OXIDASE1 (*AAO1*), *AAO2*, *NITRILASE4* (*NIT4*), *YUCCA4*, *YUCCA5*, and *YUCCA6*) were upregulated under HT in H05 following treatment with water (Figure 7A). Under Zeb treatment, fewer genes were found to be up-regulated (Figure 7A). Given there were only minor changes in the expression levels of auxin biosynthesis genes, we investigated the expression of auxin signaling pathway genes. Several such genes (mostly *auxin response factors*, *ARFs*) were upregulated in plants under HT conditions treated with water, but no obvious changes were detected under Zeb treatment (Figure 7A). These results suggest that the auxin biosynthesis and signaling pathways are slightly regulated by DNA methylation under HT.

We therefore hypothesized that auxin concentrations would not change under Zeb treatment and carried out auxin assays in anthers at the anther dehiscence stage under the following treatments: HNW (H05+NT+Water), HNZ (H05+NT+Zeb), HHW (H05+HT+Water) and HHZ (H05+HT+Zeb). We found that HT stress induced auxin accumulation in the anther, but no significant changes were detected between water and Zeb treatment under NT or HT (Figure 7B). To determine whether the auxin concentration in the endothecium differed under HT vs. Zeb treatment, we investigated the distribution of auxin in the endothecium tissue of anthers at one day before anthesis (-1 DPA) via an immunohistochemical assay. As shown in Figure 7C, the controls showed no significant differences across the four treatments (Figure 7C: a-d). HT induced the accumulation of auxin in the endothecium (Figure 7C: b', d'), but Zeb treatment had no significant effect on auxin concentration (Figure 7C: a', c'). These results suggest that HT induces auxin accumulation in the endothecium and that this might cause anther indehiscence, but it is likely that HT-disrupted DNA methylation does not play a major role in this auxin-mediated process.

DISCUSSION

Global warming is increasing the mean temperature annually (Bita and Gerats, 2013), leading to HT stress to crops and resulting in male sterility and yield reductions in rice, wheat, maize and cotton (Peng et al., 2004; Tang et al., 2006; Sakata et al., 2010; Min et al., 2014). We previously showed that two cotton lines, 84021 (HT-tolerant) and

447 H05 (HT-sensitive), exhibit different male fertility phenotypes when subjected to one
448 week of HT stress. Gene expression profile analysis revealed a significant change in
449 the number of DEGs between 84021 and H05. Further analysis showed significant
450 changes in the expression of genes involved in sugar metabolism and auxin signaling
451 pathways, suggesting roles for energy metabolism and plant hormone pathways in HT
452 stress responses in cotton anthers (Min et al., 2014). However, the mechanistic basis
453 for the differential responses observed in 84021 and H05 had been unknown.

454 DNA methylation regulates gene expression through transcriptional gene
455 silencing (Zhang and Zhu, 2011; Popova et al., 2013; Matzke and Mosher, 2014). By
456 performing bisulfite sequencing of 84021 (HT-tolerant) and H05 (HT-sensitive) under
457 NT and HT conditions at three different stages of anther development, we
458 comprehensively analyzed the roles of DNA methylation during cotton anther
459 development in response to HT. Our results revealed several intriguing DNA
460 methylation patterns in anthers under HT. First, CG and CHG methylation sites were
461 initiated in heterochromatic regions, but CHH methylation sites were relatively
462 enriched on chromosomal arms. The hyper-methylation in the CHH context occurred
463 preferentially in the euchromatin-preferential TEs, which may have caused the
464 unusual CHH methylation pattern detected in anthers. How this CHH methylation
465 pattern is generated is still unknown. Second, few changes in CG and CHG
466 methylation were identified in HT compared to NT, while CHH methylation sites
467 changed significantly in both HT-tolerant 84021 and HT-sensitive H05 under HT. We
468 conclude that hyper-CHH methylation may play a more important role than CG and
469 CHG in the response to HT stress in anthers.

470 The methylation sites in gene bodies were predominantly in the CG context, while
471 CHG and CHH showed hyper-density at promoter regions (-2kb). There were few
472 changes in CG and CHG methylation in genic regions, including promoter (-2kb),
473 gene body and downstream regions (+2kb). Previous work indicated that disrupted
474 DNA methylation disrupts gene expression, leading to seedling lethality in rice (Hu et
475 al., 2014). Based on the consensus that CHH methylation participates in
476 transcriptional gene silencing, the small changes in CG and CHG methylation under

HT in anthers further support our hypothesis that disrupted CHH methylation under HT disrupts gene expression, leading to male sterility.

The analysis of hyper-methylation levels in the siRNA+ regions indicated that 24 nt siRNAs participate in initiating DNA methylation across the genome. Further analysis of the DSRs confirmed the function of 24 nt siRNAs in altering genome-wide CHH methylation. The expression of genes that participate in the regulation of the RdDM pathway (*RDR2*, *DCL3*, *AGO4*, *HEN1* and *DRM2*) was significantly altered under HT but showed contrary expression patterns in HT-tolerant 84021 vs. HT-sensitive H05. The changes in CHH methylation and 24 nt siRNA density correspond to the expression patterns of the genes, perhaps implying that the RdDM pathway changes under HT conditions, although how the expression levels of genes involved in RdDM exhibited different changes in different samples remains unclear.

Disordered sugar metabolism is observed in anthers subjected to HT (Min et al., 2014). Both sugar and starch are vital during male reproductive development, as they serve as important energy sources (Yui et al., 2003; Zhang et al., 2010; Zhao et al., 2010; Zhu et al., 2015). Our transcriptome and experimental analysis also showed that starch hydrolysis was enhanced when DNA methylation was suppressed. These results suggest that HT-disrupted DNA methylation enhances the expression of amylase genes and resulted in the excess of consumption of starch, leading to male sterility in H05.

ROS-dependent cellular and metabolic processes occur during anther development (Hu et al., 2011; Xie et al., 2014), and unbalanced ROS metabolism results in male sterility. In rice, ROS levels are downregulated during late anther development to protect pollen grain maturation, as supported by our H_2O_2 measurements (Hu et al., 2011). Our results show that HT-induced hypo-DNA methylation levels on the promoters of RBOH genes led to their higher expression and the generation of H_2O_2 in microspores, which was detrimental to pollen development. These results show that hypo-DNA methylation in H05 under HT alleviates the silencing of amylase and RBOH genes, leading to excessive starch hydrolysis and ROS accumulation, thereby resulting in microspore abortion. This finding indicates that disrupted DNA

methylation disrupts two different pathways to induce male sterility under HT.

In Arabidopsis, auxin treatment reduces lignification of the endothecium to induce anther dehiscence (Cecchetti et al., 2013) and can rescue male sterility in wheat and Arabidopsis (Sakata et al., 2010). Our auxin analysis showed that H05 accumulates increased levels of auxin in the endothecium under HT, which is in contrast to the results in Arabidopsis, in which auxin exerts a positive effect on male sterility. The auxin assay also showed that the suppression of DNA methylation does not cause changes in auxin concentration in H05, suggesting that DNA methylation does not participate significantly in regulating auxin biosynthesis or signaling. These results suggest that auxin acts differently in different crops under HT stress.

METHODS

Plant Materials

The cotton (*Gossypium hirsutum*) lines 84021 (HT-tolerant) and H05 (HT-sensitive) used in this study were cultivated in the greenhouse under a 14 h day/10 h night photoperiod. All buds were sampled and divided into the tetrad stage (TS, 6-7 mm), tapetum degradation stage (TDS, 9-14 mm) and anther dehiscence stage (ADS, >24 mm) by bud length (Ma et al., 2012; Min et al., 2014). The same stage of anthers from the same line were harvested, pooled in tubes, and stored in liquid nitrogen or at -70°C immediately for future use.

HT Treatment Procedures and *in vitro* Application of the DNA Methylation Inhibitor Zebularine

84021 and H05 were planted in the greenhouse for various treatments. Plants under NT (29-35°C daytime and 25-28°C at night) were used for the negative control. For HT treatment, plants were moved to a greenhouse with temperatures of 39-41°C in the daytime and 29-31°C at night.

The DNA methylation inhibitor Zebularine (Zeb) (Selleck #Catalog No.S7113) was dissolved in distilled water and sprayed onto buds to suppress DNA methylation. To evaluate the most suitable concentration of Zeb for use, a graded solution series (100 μM, 150 μM, 200 μM and 250 μM) was applied to H05 under either NT or HT

conditions. Because all buds of H05 dropped after 200 μM and 250 μM Zeb treatment under NT, 150 μM Zeb was chosen for methylation suppression treatments under both NT and HT. 150 μM Zeb solution were sprayed onto all buds under NT conditions. 5 days later, half the plants were treated with HT, while the other half remained under NT. Plants cultivated under the same conditions and treated with distilled water were used as a control. The samples from different batches under HT or zebularine treatment were stored separately as different biological replicates.

DNA Extraction, Bisulfite Treatment and Library Construction

The anthers from two different batches under HT or zebularine treatment were used for DNA extraction, which was regarded as two biological replicates. Total DNA was extracted using a Plant Genomic DNA Kit (Tiangen cat# DP305). ca. 3 μg DNA was collected for bisulfite-conversion using an EZ DNA Methylation-Gold™ Kit (ZYMO RESEARCH cat# D5005) (http://www.zymoresearch.com/epigenetics/dna-methylation/bisulfite-conversion/ez-dna-methylation-gold-kit). Illumina sequencing libraries were constructed using a TruSeq DNA Methylation Kit following the manufacturer's instructions (https://www.illumina.com/products/by-type/sequencing-kits/library-prep-kits/truseq-dna-methylation.html). Unmethylated Lambda genomic DNA (Promega) was used as a control; the Lambda DNA was treated each time anther libraries were constructed. The treated lambda DNA was sequenced together with the anther library to evaluate the conversion rate. The false methylation rate of each replicates per sample was evaluated by analyzing the methylation levels of mitochondrion (Liu et al., 2013). Sequencing was performed on the Illumina HiSeq 2000 platform.

DNA Methylation Data Analysis

Low-quality sequence data for 84021, H05 and Lambda DNA were trimmed using Trimmomatic software (Bolger et al., 2014). Bisulfite non-conversion rates (0.003 of CG, 0.003 of CHG and 0.003 of CHH) were evaluated by resequencing the BS-treated lambda DNA (Yong-Villalobos et al., 2015; Zhang et al., 2015a; Wang et al., 2016) (Supplemental Table 2).

Two biological replicates of clean reads of 84021 and H05 were mapped to the

TM-1 genome using Bismark software (Krueger and Andrews, 2011) with the parameters –N 1 –L 30. The paired-end reads that uniquely mapped to the genome were reserved for further analysis. MethylKit software was utilized to evaluate the correlation between two replications of each sample (Akalin et al., 2012). The cytosines that were detected in two sets of BS-data were selected to identify putative methylated cytosines (mCs). Putative mCs were extracted using bismark_methylation_extractor software with the parameters --no_overlap --CX_context. All putative mCs were pooled into the classic binomial test with a cut-off p-value <1e-4. True mCs were determined based on p-value under the binomial distribution $p = (mCs, totalCs, error\_rate)$, where mCs = number of mCs; totalCs = mCs + unmethylated Cs; error_rate is the error rate for the nonconversion rate of the Lambda DNA.

For DMR calling, the whole genome was divided into 100 bp bins with no overlap, and all mCs identified by binomial test in two replicates were mapped to 100 bp bins. Fisher's Exact test was then performed with the cutoff at 0.05 (Ausin et al., 2012; Calarco et al., 2012; Guo et al., 2014; Zhang et al., 2015a; Groth et al., 2016; Wang et al., 2016). Multiple testing correction (FDR < 0.05) was subsequently followed to test each window.

Small RNA Library Preparation and Sequencing

A total of 10 μg RNA from each sample was prepared using a modified Guanidine Thiocyanate method (Min et al., 2013), and 5S sections of RNA were separated by agarose gel electrophoresis. Small RNA libraries were constructed using TruSeq Small RNA Library Preparation Kits (Illumina) following the manufacturer's protocol, with two biological replicates. Clean reads (18-26 bp) were obtained after adapter clipping and raw data trimming. Structural RNAs such as rRNA, snRNA, tRNA were filtered via alignment to Rfam (http://rfam.xfam.org/), and the miRBase (http://www.mirbase.org/) database was used to predict putative microRNAs.

All remaining reads were mapped to the cotton genome using Bowtie (version 1.1.1) (Langmead et al., 2009), allowing no mismatches (-a -v 0 -m 200). Only 24 nt

siRNAs that uniquely mapped to the genome, with no overlaps with each other, were selected for further analysis.

RNA-seq and Data Analysis

Anthers from two different batches under HT treatment were sampled for RNA extraction. Total RNA was extracted using a modified Guanidine Thiocyanate method (Min et al., 2013). Approximately 3 μg RNA was used to construct libraries with a TruSeq Stranded Total RNA Kit with two biological replicates per sample (https://www.illumina.com/techniques/sequencing/rna-sequencing/total-rna-seq.html). Adapters and low-quality reads were clipped using Trimmomatic software (Bolger et al., 2014). All remaining reads were mapped to the cotton genome using TopHat2 (Ghosh and Chan, 2016). Further identification of DEGs was performed using Cuffdiff software with a cutoff p-value <0.05 (Ghosh and Chan, 2016).

Tissue Sectioning, Staining and Imaging

Bracts and petals were removed from buds, which were subsequently immersed in 50% FAA (50 mL absolute ethanol, 10 mL 37% formaldehyde solution, 5 mL acetic acid and diluted with water to 100 mL) and vacuum infiltrated three times for 15 min to fix the tissue. After infiltration, the solution was replaced with fresh FAA solution and postfixed at 4°C for at least 12 h. Fixed samples were dehydrated using a graded ethanol series (30%, 50%, 70%, 95% and 100%) for 1 h at each concentration and embedded in paraffin. Embedded tissues were sectioned to 10 μm thickness. Toluidine blue solution (1%) and aniline blue solution (1%) were used to stain the anther sections. A Zeiss Axio Scope A1 microscope was used to image the samples under bright field for Toluidine Blue staining and at 395 nm excitation for aniline blue staining.

ROS and Starch Staining of Pollen Grains

Pollen from different treatments including H05+NT+Water (HNW; H, H05; N, normal temperature; W, water), H05+HT+Water (HHW; H, H05; H, high temperature; W, water), H05+NT+Zeb (HNZ; H, H05; N, normal temperature; Zeb, Zebularine) and H05+HT+Zeb (HHZ; H, H05; H, high temperature; Zeb, Zebularine) were stained for ROS and starch detection. Flowers on the day of blooming were carefully

harvested, the petals were quickly removed, and the samples were immediately immersed in PBS (Phosphate Buffer Solution, pH=7, prepared in 15 mL tubes and previously stored at room temperature) to avoid generating a ROS burst during the release of pollen grains. HT treatment was performed in an incubator for 2 hours. Flowers under NT conditions were used as a negative control. After treatment, the pollen was incubated for 30 min in the dark in 10 μM 2',7'-dichlorodihydrofluorescein diacetate (2',7'-DCFDA) dissolved in PBS for ROS staining. Samples were washed twice in PBS before imaging at excitation wavelength 488 nm and emission wavelength 522 nm (Tang et al., 2014).

I_2-KI solution was used for starch staining in pollen. Samples were washed in PBS after staining in I_2-KI solution for 3 minutes, and images were taken under bright field.

ROS Quantification

Anthers were collected in 2 mL tubes, ground and extracted using 80% acetone for approximately 30 minutes in the dark at 4℃. ROS quantification was performed using a H_2O_2 Quantitative Assay Kit (Sangon Biotech # C500069-0250), with at least 5 biological replicates (samples from different experiments) and 2 technological replicates (samples from the experiment) for each sample. Concentrations were calculated as μmol/g fresh weight (FW).

Plant Hormone Measurements

Approximately 50 mg anther tissue was sampled and stored in 2 mL tubes, ground using iron balls, and extracted using 80% methanol by shaking at 4℃ overnight. Plant hormone measurements were performed on an Agilent 4000Q-TRAR HPLC-MS system, with 3-IAA (Sigma # 87-51-4) used as the internal standard.

Soluble Sugar and Starch Measurements

Soluble sugar was extracted using 80% acetone as described for ROS quantification, and the sediment was collected to measure starch content. Total soluble sugar was determined following the anthrone-sulfuric acid method (Min et al., 2014). Starch measurements were performed via perchloric acid hydrolysis of starch-anthrone sulfuric acid (Min et al., 2014). Both soluble sugar and starch contents were

calculated as mg/g fresh weight (FW).

Immunohistochemical Assay of IAA

An immunohistochemical assay of IAA was performed as described previously (Hou and Huang, 2005). IAA in anthers was fixed with carbodiimide hydrochloride (EDAC, Sangon # C600433) under a vacuum for 1 h, followed by 50% FAA. Before immunochemistry, anthers were incubated in blocking solution (10 mM Phosphate Buffer Solution, PBS, pH=7.2; 0.1% Tween-20; 1.5% Glycine and 5% Bovine Serum Albumin, BSA, Biosharp # BS043E) for 45 minutes, and IAA antibody (Sigma # A0855-200UL) diluted in PBS/BSA (10 mM PBS; 0.8% BSA) as the primary antibody was incubated with the tissue sections. Tissue sections were incubated with an alkaline phosphatase secondary antibody, covered with Parafilm and incubated with Western Blue® Stabilized Substrate for Alkaline Phosphatase (Promega # S3841). Incubation was stopped by washing in water or PBS, and the sections were mounted on a cover glass before imagining. Sections incubated with anti-mouse IgG diluted (Promega # S3721) in PBS/BSA acted as a negative control.

qRT-PCR

For qRT-PCR, 3 μg RNA was reverse-transcribed using M-MLV (Promega) following the manufacturer's protocol. qRT-PCR was performed using an ABI 7500 RealTime PCR system. Relative gene expression levels were calculated using the $2^{-\Delta Ct}$ method as previously described (Min et al., 2014). Expression levels were normalized to *GhUBIQUITIN7* as an internal control to standardize RNA content.

Accession Numbers

Sequence data from this article can be found in the GenBank/EMBL libraries under the following accession numbers:

GhUBIQUITIN7 (*DQ116441*); *GhRDR2* (*Gh_A12G2496*); *GhRDR2* (*Gh_A13G0247*) *GhDCL3* (*Gh_D13G2027*); *GhHEN1* (*Gh_A06G1061*); *GhAGO4* (*Gh_D07G1699*); *GhAGO4* (*Gh_A07G1540*); *GhAGO4* (*Gh_A08G1752*); *GhDRM2* (*Gh_A09G0264*).

The whole genome bisulfite sequencing reads, small RNA sequencing reads, and RNA-sequencing reads have been deposited with the National Center for

686 Biotechnology Information under Sequence Read Archive (SRA) accession number
687 PRJNA393079.
688 The profiles of DNA methylation and gene expression levels of 84021 and H05 under
689 NT and HT are presented in the website:
690 http://cgrd.hzau.edu.cn/cgi-bin/gb2/gbrowse/CottonReSequencing2016/
691
692 **Supplemental Data**
693 **Supplemental Figure 1.** Correlation analysis of the replicates of each sample using
694 methylKit software.
695 **Supplemental Figure 2.** Number of methylated cytosines (mCs) identified by
696 BS-seq.
697 **Supplemental Figure 3.** Methylation levels of methylated cytosines (mCs) identified
698 by binomial tests.
699 **Supplemental Figure 4.** Fraction of mCs to total cytosines genome wide .
700 **Supplemental Figure 5.** Circos plots showing the distribution of methylated
701 cytosines (mCs) in the CG, CHG and CHH contexts and 24nt siRNAs on all 26
702 chromosomes.
703 **Supplemental Figure 6.** Circos plots showing the distribution of CG and CHG
704 DMRs under high temperature (HT) conditions in 84021 (HT-tolerant) and H05
705 (HT-sensitive) at the tetrad stage (TS), tapetum degradation stage (TDS) and anther
706 dehiscence stage (ADS).
707 **Supplemental Figure 7.** Correlation matrix between CHH methylation level, number
708 of 24 nt siRNAs, number of genes and number of TEs in 1 M regions.
709 **Supplemental Figure 8.** Expression levels of several RdDM pathway genes in 84021
710 (HT-tolerant) and H05 (HT-sensitive) at the tetrad stage (TS), tapetum degradation
711 stage (TDS) and anther dehiscence stage (ADS).
712 **Supplemental Figure 9.** CG and CHG methylation levels in gene regions including
713 promoters (-2kb), gene bodies and downstream regions (+2kb) in 84021 (HT-tolerant)
714 and H05 (HT-sensitive).
715 **Supplemental Figure 10.** Statistics of differentially methylated regions (DMRs)

716 mapping of gene regions including promoter (-2kb), gene bodies and downstream
717 regions (+2kb) in the CG, CHG and CHH contexts.
718 **Supplemental Figure 11.** Changes in DNA methylation levels in the CG, CHG and
719 CHH contexts under Zebularine treatment.
720 **Supplemental Figure 12.** Number of differentially expressed genes (DEGs) in H05
721 (HT-sensitive) treated with Zebularine under normal temperature (NT) and high
722 temperature (HT) conditions at the tetrad stage (TS), tapetum degradation stage (TDS)
723 and anther dehiscence stage (ADS).
724 **Supplemental Figure 13.** Gene ontology (GO) analysis of differentially expressed
725 genes (DEGs) identified under HT or Zebularine treatment.
726 **Supplemental Table 1.** Bisulfite sequencing (BS-seq) data analysis.
727 **Supplemental Table 2.** Bisulfite non-conversion rate analysis.
728 **Supplemental Table 3.** Methylation status of cotton mitochondrial genomes
729 determined by BS-seq.
730 **Supplemental Table 4.** Number of methylated cytosines (mCs) identified by BS-seq.
731 **Supplemental Table 5.** Number of DMRs in the CG, CHG and CHH contexts.
732 **Supplemental Table 6.** Statistical analysis of small RNA sequencing data.
733 **Supplemental Table 7.** Bisulfite sequencing (BS-seq) data for Zebularine-treated
734 samples.
735 **Supplemental Table 8.** RNA sequencing data analysis.
736 **Supplemental Table 9.** Summary of differentially transcribed TEs.
737 **Supplemental Table 10.** Summary of differentially expressed genes.
738 **Supplemental Table 11.** Primers used in this work.
739 **Supplemental Data Set 1.** Number of short, medium and long TEs in each 1 Mb
740 genomic region.
741 **Supplemental Data Set 2.** DMR information about CG context with FDR.
742 **Supplemental Data Set 3.** DMR information about CHG context with FDR.
743 **Supplemental Data Set 4.** DMRs information about CHH context with FDR.
744
745 **ACKNOWLEDGEMENTS**

The funding support by China Agriculture Research System (CARS-18-09) and the National Key Research and Development Program of China (2016YFD0101402) is appreciated. We are also grateful to Dr. Hongbo Liu (Huazhong Agricultural University, China) for assistance with liquid chromatography/mass spectrometry analysis.

AUTHOR CONTRIBUTIONS

X.Z. and L.M. conceived and designed the experiments. Y.M., L.M., Y.L., Y.W., Y.D., X.S. and Q.H. performed HT treatment. Y.M. and Y.W. performed tissue section, pollen staining and imaging. Y.M., C.W., Y.Z., and Q.F. measured soluble sugar, starch and ROS contents. Q.Z. constructed the Illumina sequencing libraries. Y.M. and M.W. contributed to data analysis. Y.M. wrote the article, L.M and X.Z. revised it.

References

Akalin, A., Kormaksson, M., Li, S., Garrett-Bakelman, F. E., Figueroa, M. E., Melnick, A., Mason, C. E. (2012). methylKit: a comprehensive R package for the analysis of genome-wide DNA methylation profiles. Genome Biol**. 13**, R87

Ausin, I., Greenberg, M.V., Simanshu, D.K., Hale, C.J., Vashisht, A.A., Simon, S.A., Lee, T.F., Feng, S., Espanola, S.D., Meyers, B.C., Wohlschlegel, J.A., Patel, D.J., and Jacobsen, S.E. (2012). INVOLVED IN DE NOVO 2-containing complex involved in RNA-directed DNA methylation in Arabidopsis. Proc Natl Acad Sci U S A. **109,** 8374-8381.

Bita, C.E., and Gerats, T. (2013). Plant tolerance to high temperature in a changing environment: scientific fundamentals and production of heat stress-tolerant crops. Front Plant Sci. **4,** 273.

Bolger, A.M., Lohse, M., and Usadel, B. (2014). Trimmomatic: a flexible trimmer for Illumina sequence data. Bioinformatics. **30,** 2114-2120.

Calarco, J.P., Borges, F., Donoghue, M.T., Van Ex, F., Jullien, P.E., Lopes, T., Gardner, R., Berger, F., Feijo, J.A., Becker, J.D., and Martienssen, R.A. (2012). Reprogramming of DNA methylation in pollen guides epigenetic inheritance via small RNA. Cell. **151,** 194-205.

Cao, X., and Jacobsen, S.E. (2002). Locus-specific control of asymmetric and CpNpG methylation by the DRM and CMT3 methyltransferase genes. Proc Natl Acad Sci U S A. **99 Suppl 4,** 16491-16498.

Cao, X.F., Aufsatz, W., Zilberman, D., Mette, M.F., Huang, M.S., Matzke, M., and Jacobsen, S.E. (2003). Role of the DRM and CMT3 Methyltransferases in RNA-directed DNA methylation. Curr Biol. **13,** 2212-2217.

Cecchetti, V., Altamura, M.M., Falasca, G., Costantino, P., and Cardarelli, M. (2008). Auxin regulates Arabidopsis anther dehiscence, pollen maturation, and filament elongation. Plant

Cell. **20,** 1760-1774.

Cecchetti, V., Celebrin, D., Napoli, N., Ghelli, R., Brunetti, P., Costantino, P., and Cardarelli, M. (2017). An auxin maximum in the middle layer controls stamen development and pollen maturation in Arabidopsis. New Phytol. **213,** 1194-1207.

Cecchetti, V., Altamura, M.M., Brunetti, P., Petrocelli, V., Falasca, G., Ljung, K., Costantino, P., and Cardarelli, M. (2013). Auxin controls Arabidopsis anther dehiscence by regulating endothecium lignification and jasmonic acid biosynthesis. Plant J. **74,** 411-422.

Chan, S.W., Zilberman, D., Xie, Z., Johansen, L.K., Carrington, J.C., and Jacobsen, S.E. (2004). RNA silencing genes control de novo DNA methylation. Science. **303,** 1336.

Gardiner, L.J., Quinton-Tulloch, M., Olohan, L., Price, J., Hall, N., and Hall, A. (2015). A genome-wide survey of DNA methylation in hexaploid wheat. Genome Biol. **16,** 273.

Gent, J.I., Madzima, T.F., Bader, R., Kent, M.R., Zhang, X., Stam, M., McGinnis, K.M., and Dawe, R.K. (2014). Accessible DNA and relative depletion of H3K9me2 at maize loci undergoing RNA-directed DNA methylation. Plant Cell. **26,** 4903-4917.

Ghosh, S., and Chan, C.K. (2016). Analysis of RNA-Seq Data Using TopHat and Cufflinks. Methods Mol Biol. **1374,** 339-361.

Groth, M., Moissiard, G., Wirtz, M., Wang, H., Garcia-Salinas, C., Ramos-Parra, P.A., Bischof, S., Feng, S., Cokus, S.J., John, A., Smith, D.C., Zhai, J., Hale, C.J., Long, J.A., Hell, R., Diaz de la Garza, R.I., and Jacobsen, S.E. (2016). MTHFD1 controls DNA methylation in Arabidopsis. Nat Commun. **7,** 11640.

Guo, H., Zhu, P., Yan, L., Li, R., Hu, B., Lian, Y., Yan, J., Ren, X., Lin, S., Li, J., Jin, X., Shi, X., Liu, P., Wang, X., Wang, W., Wei, Y., Li, X., Guo, F., Wu, X., Fan, X., Yong, J., Wen, L., Xie, S.X., Tang, F., and Qiao, J. (2014). The DNA methylation landscape of human early embryos. Nature. **511,** 606-610.

Havecker, E.R., Wallbridge, L.M., Hardcastle, T.J., Bush, M.S., Kelly, K.A., Dunn, R.M., Schwach, F., Doonan, J.H., and Baulcombe, D.C. (2010). The Arabidopsis RNA-directed DNA methylation argonautes functionally diverge based on their expression and interaction with target loci. Plant Cell. **22,** 321-334.

He, X.J., Chen, T., and Zhu, J.K. (2011). Regulation and function of DNA methylation in plants and animals. Cell Res. **21,** 442-465.

Henderson, I.R., and Jacobsen, S.E. (2007). Epigenetic inheritance in plants. Nature **447,** 418-424.

Hou, Z.X., and Huang, W.D. (2005). Immunohistochemical localization of IAA and ABP1 in strawberry shoot apexes during floral induction. Planta. **222,** 678-687.

Hu, L., Liang, W., Yin, C., Cui, X., Zong, J., Wang, X., Hu, J., and Zhang, D. (2011). Rice MADS3 regulates ROS homeostasis during late anther development. Plant Cell. **23,** 515-533.

Hu, L., Li, N., Xu, C., Zhong, S., Lin, X., Yang, J., Zhou, T., Yuliang, A., Wu, Y., Chen, Y.R., Cao, X., Zemach, A., Rustgi, S., von Wettstein, D., and Liu, B. (2014). Mutation of a major CG methylase in rice causes genome-wide hypomethylation, dysregulated genome expression, and seedling lethality. Proc Natl Acad Sci U S A. **111,** 10642-10647.

Iwasaki, M., and Paszkowski, J. (2014). Identification of genes preventing transgenerational transmission of stress-induced epigenetic states. Proc Natl Acad Sci U S A. **111,** 8547-8552.

Jia, Y., Lisch, D.R., Ohtsu, K., Scanlon, M.J., Nettleton, D., and Schnable, P.S. (2009). Loss of RNA-dependent RNA polymerase 2 (RDR2) function causes widespread and unexpected changes in the expression of transposons, genes, and 24-nt small RNAs. PLoS Genet. **5,**

827 e1000737.
828 **Jiang, C., Mithani, A., Belfield, E.J., Mott, R., Hurst, L.D., and Harberd, N.P.** (2014).
829 Environmentally responsive genome-wide accumulation of de novo Arabidopsis thaliana
830 mutations and epimutations. Genome Res. **24,** 1821-1829.
831 **Jullien, P.E., Susaki, D., Yelagandula, R., Higashiyama, T., and Berger, F.** (2012). DNA
832 methylation dynamics during sexual reproduction in Arabidopsis thaliana. Curr Biol. **22,**
833 1825-1830.
834 **Kim, D.H., Doyle, M.R., Sung, S., and Amasino, R.M.** (2009). Vernalization: winter and the timing
835 of flowering in plants. Annu Rev Cell Dev Biol. **25,** 277-299.
836 **Krueger, F., and Andrews, S.R.** (2011). Bismark: a flexible aligner and methylation caller for
837 Bisulfite-Seq applications. Bioinformatics. **27,** 1571-1572.
838 **Langmead, B., Trapnell, C., Pop, M., and Salzberg, S.L.** (2009). Ultrafast and memory-efficient
839 alignment of short DNA sequences to the human genome. Genome Biol. **10,** R25.
840 **Law, J.A., and Jacobsen, S.E.** (2010). Establishing, maintaining and modifying DNA methylation
841 patterns in plants and animals. Nat Rev Genet. **11,** 204-220.
842 **Le, T.N., Schumann, U., Smith, N.A., Tiwari, S., Au, P.C., Zhu, Q.H., Taylor, J.M., Kazan, K.,**
843 **Llewellyn, D.J., Zhang, R., Dennis, E.S., and Wang, M.B.** (2014). DNA demethylases
844 target promoter transposable elements to positively regulate stress responsive genes in
845 Arabidopsis. Genome Biol. **15,** 458.
846 **Li, Q., Gent, J.I., Zynda, G., Song, J., Makarevitch, I., Hirsch, C.D., Hirsch, C.N., Dawe, R.K.,**
847 **Madzima, T.F., McGinnis, K.M., Lisch, D., Schmitz, R.J., Vaughn, M.W., and Springer,**
848 **N.M.** (2015). RNA-directed DNA methylation enforces boundaries between heterochromatin
849 and euchromatin in the maize genome. Proc Natl Acad Sci U S A. **112,** 14728-14733.
850 **Liu, G., Cao, D., Li, S., Su, A., Geng, J., Grover, C.E., Hu, S., and Hua, J.** (2013). The complete
851 mitochondrial genome of Gossypium hirsutum and evolutionary analysis of higher plant
852 mitochondrial genomes. Plos One **8,** e69476.
853 **Ma, J., Wei, H., Song, M., Pang, C., Liu, J., Wang, L., Zhang, J., Fan, S., and Yu, S.** (2012).
854 Transcriptome profiling analysis reveals that flavonoid and ascorbate-glutathione cycle are
855 important during anther development in Upland cotton. Plos One. **7,** e49244.
856 **Marino, D., Dunand, C., Puppo, A., and Pauly, N.** (2012). A burst of plant NADPH oxidases.
857 Trends Plant Sci. **17,** 9-15.
858 **Matzke, M.A., and Mosher, R.A.** (2014). RNA-directed DNA methylation: an epigenetic pathway of
859 increasing complexity. Nat Rev Genet. **15,** 394-408.
860 **Melnyk, C.W., Molnar, A., Bassett, A., and Baulcombe, D.C.** (2011). Mobile 24 nt small RNAs
861 direct transcriptional gene silencing in the root meristems of Arabidopsis thaliana. Curr Biol.
862 **21,** 1678-1683.
863 **Min, L., Zhu, L., Tu, L., Deng, F., Yuan, D., and Zhang, X.** (2013). Cotton GhCKI disrupts normal
864 male reproduction by delaying tapetum programmed cell death via inactivating starch
865 synthase. Plant J. **75,** 823-835.
866 **Min, L., Li, Y., Hu, Q., Zhu, L., Gao, W., Wu, Y., Ding, Y., Liu, S., Yang, X., and Zhang, X.**
867 (2014). Sugar and auxin signaling pathways respond to high-temperature stress during anther
868 development as revealed by transcript profiling analysis in cotton. Plant Physiol. **164,**
869 1293-1308.
870 **Mitsuda, N., Seki, M., Shinozaki, K., and Ohme-Takagi, M.** (2005). The NAC transcription factors

NST1 and NST2 of Arabidopsis regulate secondary wall thickenings and are required for anther dehiscence. Plant Cell. **17,** 2993-3006.

Mittler, R., Vanderauwera, S., Gollery, M., and Van Breusegem, F. (2004). Reactive oxygen gene network of plants. Trends Plant Sci. **9,** 490-498.

Pecinka, A., Dinh, H.Q., Baubec, T., Rosa, M., Lettner, N., and Mittelsten Scheid, O. (2010). Epigenetic regulation of repetitive elements is attenuated by prolonged heat stress in Arabidopsis. Plant Cell. **22,** 3118-3129.

Peng, S., Huang, J., Sheehy, J.E., Laza, R.C., Visperas, R.M., Zhong, X., Centeno, G.S., Khush, G.S., and Cassman, K.G. (2004). Rice yields decline with higher night temperature from global warming. Proc Natl Acad Sci U S A. **101,** 9971-9975.

Popova, O.V., Dinh, H.Q., Aufsatz, W., and Jonak, C. (2013). The RdDM pathway is required for basal heat tolerance in Arabidopsis. Mol Plant. **6,** 396-410.

Rigal, M., Becker, C., Pelissier, T., Pogorelcnik, R., Devos, J., Ikeda, Y., Weigel, D., and Mathieu, O. (2016). Epigenome confrontation triggers immediate reprogramming of DNA methylation and transposon silencing in Arabidopsis thaliana F1 epihybrids. Proc Natl Acad Sci U S A. **113,** E2083-2092.

Sakata, T., Oshino, T., Miura, S., Tomabechi, M., Tsunaga, Y., Higashitani, N., Miyazawa, Y., Takahashi, H., Watanabe, M., and Higashitani, A. (2010). Auxins reverse plant male sterility caused by high temperatures. Proc Natl Acad Sci U S A. **107,** 8569-8574.

Secco, D., Wang, C., Shou, H., Schultz, M.D., Chiarenza, S., Nussaume, L., Ecker, J.R., Whelan, J., and Lister, R. (2015). Stress induced gene expression drives transient DNA methylation changes at adjacent repetitive elements. Elife. **4**.

Shen, X., De Jonge, J., Forsberg, S.K., Pettersson, M.E., Sheng, Z., Hennig, L., and Carlborg, O. (2014). Natural CMT2 variation is associated with genome-wide methylation changes and temperature seasonality. PLoS Genet. **10,** e1004842.

Sijen, T., Vijn, I., Rebocho, A., van Blokland, R., Roelofs, D., Mol, J.N., and Kooter, J.M. (2001). Transcriptional and posttranscriptional gene silencing are mechanistically related. Curr Biol. **11,** 436-440.

Slotkin, R.K., Vaughn, M., Borges, F., Tanurdzic, M., Becker, J.D., Feijo, J.A., and Martienssen, R.A. (2009). Epigenetic reprogramming and small RNA silencing of transposable elements in pollen. Cell. **136,** 461-472.

Song, Q.X., Lu, X., Li, Q.T., Chen, H., Hu, X.Y., Ma, B., Zhang, W.K., Chen, S.Y., and Zhang, J.S. (2013). Genome-wide analysis of DNA methylation in soybean. Mol Plant. **6,** 1961-1974.

Stromme, C.B., Julkunen-Tiitto, R., Krishna, U., Lavola, A., Olsen, J.E., and Nybakken, L. (2015). UV-B and temperature enhancement affect spring and autumn phenology in Populus tremula. Plant Cell Environ. **38,** 867-877.

Tang, J.H., Fu, Z.Y., Hu, Y.M., Li, J.S., Sun, L.L., and Ji, H.Q. (2006). Genetic analyses and mapping of a new thermo-sensitive genic male sterile gene in maize. Theor Appl Genet. **113,** 11-15.

Tang, W., Tu, L., Yang, X., Tan, J., Deng, F., Hao, J., Guo, K., Lindsey, K., and Zhang, X. (2014). The calcium sensor GhCaM7 promotes cotton fiber elongation by modulating reactive oxygen species (ROS) production. New Phytol. **202,** 509-520.

Wang, M., Wang, P., Tu, L., Zhu, S., Zhang, L., Li, Z., Zhang, Q., Yuan, D., and Zhang, X. (2016). Multi-omics maps of cotton fibre reveal epigenetic basis for staged single-cell

differentiation. Nucleic Acids Res. **44,** 4067-4079.

Wang, S., Chen, J., Zhang, W., Hu, Y., Chang, L., Fang, L., Wang, Q., Lv, F., Wu, H., Si, Z., Chen, S., Cai, C., Zhu, X., Zhou, B., Guo, W., and Zhang, T. (2015). Sequence-based ultra-dense genetic and physical maps reveal structural variations of allopolyploid cotton genomes. Genome Biol. **16,** 108.

Wicker, T., Sabot, F., Hua-Van, A., Bennetzen, J.L., Capy, P., Chalhoub, B., Flavell, A., Leroy, P., Morgante, M., Panaud, O., Paux, E., SanMiguel, P., and Schulman, A.H. (2007). A unified classification system for eukaryotic transposable elements. Nat Rev Genet. **8,** 973-982.

Xie, H.T., Wan, Z.Y., Li, S., and Zhang, Y. (2014). Spatiotemporal Production of Reactive Oxygen Species by NADPH Oxidase Is Critical for Tapetal Programmed Cell Death and Pollen Development in Arabidopsis. Plant Cell. **26,** 2007-2023.

Yong-Villalobos, L., Gonzalez-Morales, S.I., Wrobel, K., Gutierrez-Alanis, D., Cervantes-Perez, S.A., Hayano-Kanashiro, C., Oropeza-Aburto, A., Cruz-Ramirez, A., Martinez, O., and Herrera-Estrella, L. (2015). Methylome analysis reveals an important role for epigenetic changes in the regulation of the Arabidopsis response to phosphate starvation. Proc Natl Acad Sci U S A. **112,** E7293-7302.

Yui, R., Iketani, S., Mikami, T., and Kubo, T. (2003). Antisense inhibition of mitochondrial pyruvate dehydrogenase E1alpha subunit in anther tapetum causes male sterility. Plant J. **34,** 57-66.

Zhang, H., and Zhu, J.K. (2011). RNA-directed DNA methylation. Curr Opin Plant Biol **14,** 142-147.

Zhang, H., Liang, W., Yang, X., Luo, X., Jiang, N., Ma, H., and Zhang, D. (2010). Carbon starved anther encodes a MYB domain protein that regulates sugar partitioning required for rice pollen development. Plant Cell. **22,** 672-689.

Zhang, J., Liu, Y., Xia, E.H., Yao, Q.Y., Liu, X.D., and Gao, L.Z. (2015a). Autotetraploid rice methylome analysis reveals methylation variation of transposable elements and their effects on gene expression. Proc Natl Acad Sci U S A. **112,** E7022-7029.

Zhang, T., Hu, Y., Jiang, W., Fang, L., Guan, X., Chen, J., Zhang, J., Saski, C.A., Scheffler, B.E., Stelly, D.M., Hulse-Kemp, A.M., Wan, Q., Liu, B., Liu, C., Wang, S., Pan, M., Wang, Y., Wang, D., Ye, W., Chang, L., Zhang, W., Song, Q., Kirkbride, R.C., Chen, X., Dennis, E., Llewellyn, D.J., Peterson, D.G., Thaxton, P., Jones, D.C., Wang, Q., Xu, X., Zhang, H., Wu, H., Zhou, L., Mei, G., Chen, S., Tian, Y., Xiang, D., Li, X., Ding, J., Zuo, Q., Tao, L., Liu, Y., Li, J., Lin, Y., Hui, Y., Cao, Z., Cai, C., Zhu, X., Jiang, Z., Zhou, B., Guo, W., Li, R., and Chen, Z.J. (2015b). Sequencing of allotetraploid cotton (Gossypium hirsutum L. acc. TM-1) provides a resource for fiber improvement. Nat Biotechnol. **33,** 531-537.

Zhao, Q., Gallego-Giraldo, L., Wang, H., Zeng, Y., Ding, S.Y., Chen, F., and Dixon, R.A. (2010). An NAC transcription factor orchestrates multiple features of cell wall development in Medicago truncatula. Plant J. **63,** 100-114.

Zhong, S., Fei, Z., Chen, Y.R., Zheng, Y., Huang, M., Vrebalov, J., McQuinn, R., Gapper, N., Liu, B., Xiang, J., Shao, Y., and Giovannoni, J.J. (2013). Single-base resolution methylomes of tomato fruit development reveal epigenome modifications associated with ripening. Nat Biotechnol. **31,** 154-159.

Zhu, X., Liang, W., Cui, X., Chen, M., Yin, C., Luo, Z., Zhu, J., Lucas, W.J., Wang, Z., and Zhang, D. (2015). Brassinosteroids promote development of rice pollen grains and seeds by triggering expression of Carbon Starved Anther, a MYB domain protein. Plant J. **82,** 570-581.

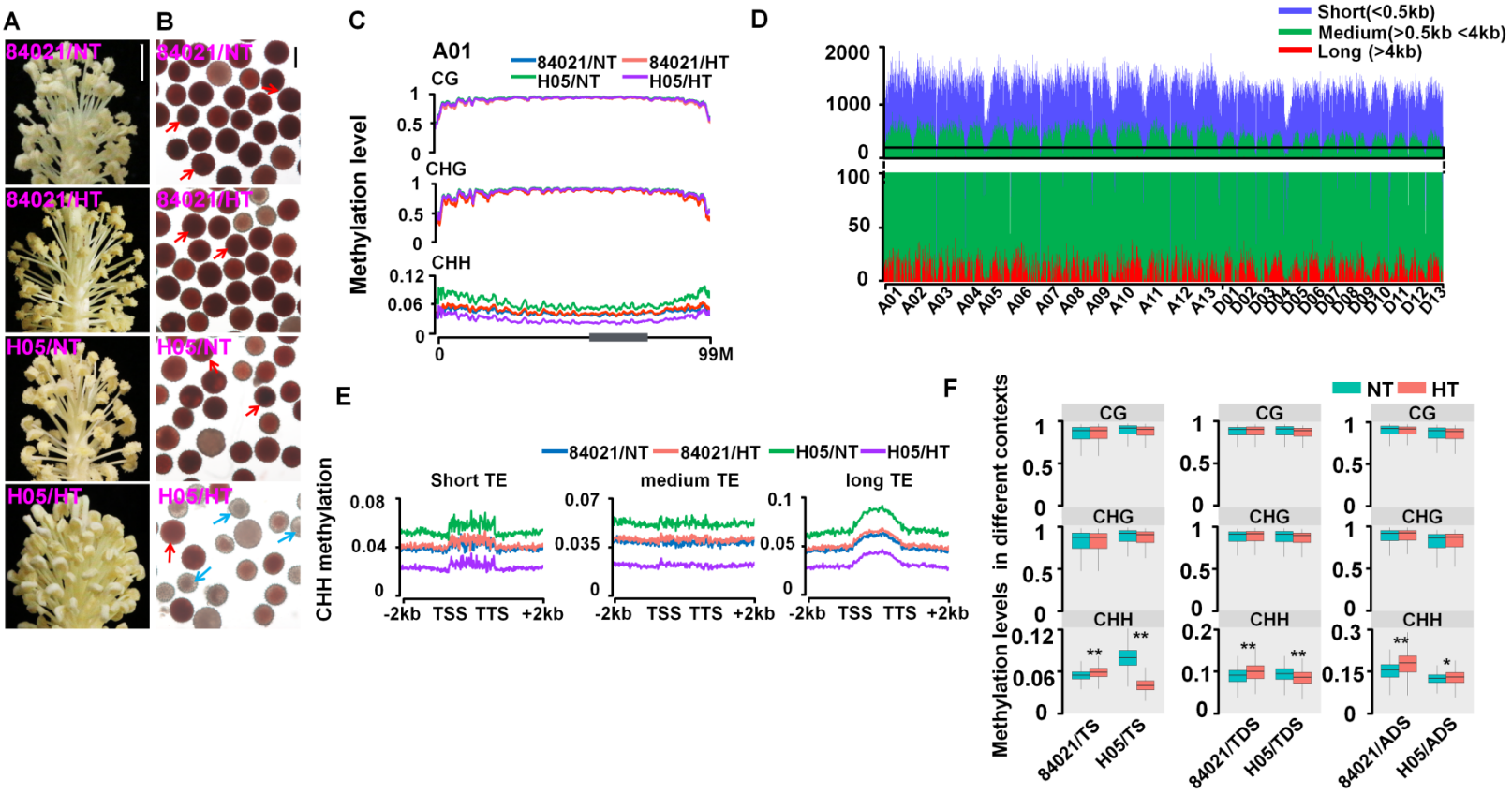

Figure 1. Male fertility phenotypes and DNA methylation patterns during anther development under high temperature (HT) stress.
(A) At the anther dehiscence stage (ADS), both 84021 and H05 released pollen grains normally under normal temperature (NT). Under high temperature (HT), 84021 dehisced normally while H05 showed indehiscence. Bar=5 mm.
(B) 2,3,5-Triphenylterzolium (TTC) staining of pollen in 84021 and H05 under NT and HT. Both 84021 and H05 produced normal pollen (red arrows) under NT. Under HT, 84021 produced normal pollen, while H05 produced sterile pollen (blue arrows). Bar=50 μm.
(C) Distribution of CG, CHG and CHH methylation sites on chromosome A01 in 84021 under NT (blue lines), H05 under NT (green lines), 84021 under HT (red lines) and H05 under HT (purple lines) at the tetrad stage. CG and CHG methylation sites were enriched in heterochromatic regions, while CHH methylation sites were relatively enriched in euchromatic regions. Significant changes in CHH methylation occurred, while CG and CHG remained stable under HT on a chromosome-wide scale. The approximate centromere regions are indicated by a gray rectangle. The Y-axis shows the relative methylation levels calculated as the number of mCs / number of total Cs (%) in each 1 Mb genomic region.
(D) Distribution of short (<0.5kb, blue columns), medium (0.5–4kb, green columns) and long (>4kb, red columns) TEs on each chromosome. The X-axis shows the *Gossypium hirsutum* chromosome numbers, and the Y-axis shows the number of each type of TE in every 1 Mb region of each chromosome. Short TEs occupy a large proportion of total TEs. Long TEs are relatively rare and are spread uniformly on each chromosome.
(E) CHH methylation levels in 84021 under NT (blue lines), H05 under NT (green lines), 84021 under HT (red lines) and H05 under HT (purple lines) on short, medium and long TEs at the tetrad stage. Short and long TEs showed hyper-CHH methylation in TE bodies compared to upstream (-2kb) and downstream (+2kb) regions, while medium TEs showed only slight changes in CHH methylation.
(F) CG and CHG showed little change on a genome-wide scale under HT, while CHH changed significantly under HT. 84021 showed hyper-CHH methylation at the tetrad stage (TS), tapetum degradation stage (TDS) and anther dehiscence stage (ADS) under HT. H05 showed hypo-CHH methylation at the tetrad stage (TS) and tapetum degradation stage (TDS) while displaying hyper-CHH methylation at the anther dehiscence stage (ADS) under HT. The comparison was performed by comparing the methylation levels of each 1Mb genomic region between NT and HT (1947 comparison pairs). *Significant difference from NT; statistical significances were determined by paired two-tailed Student's *t* tests, $p<0.05$; **$p<0.01$.

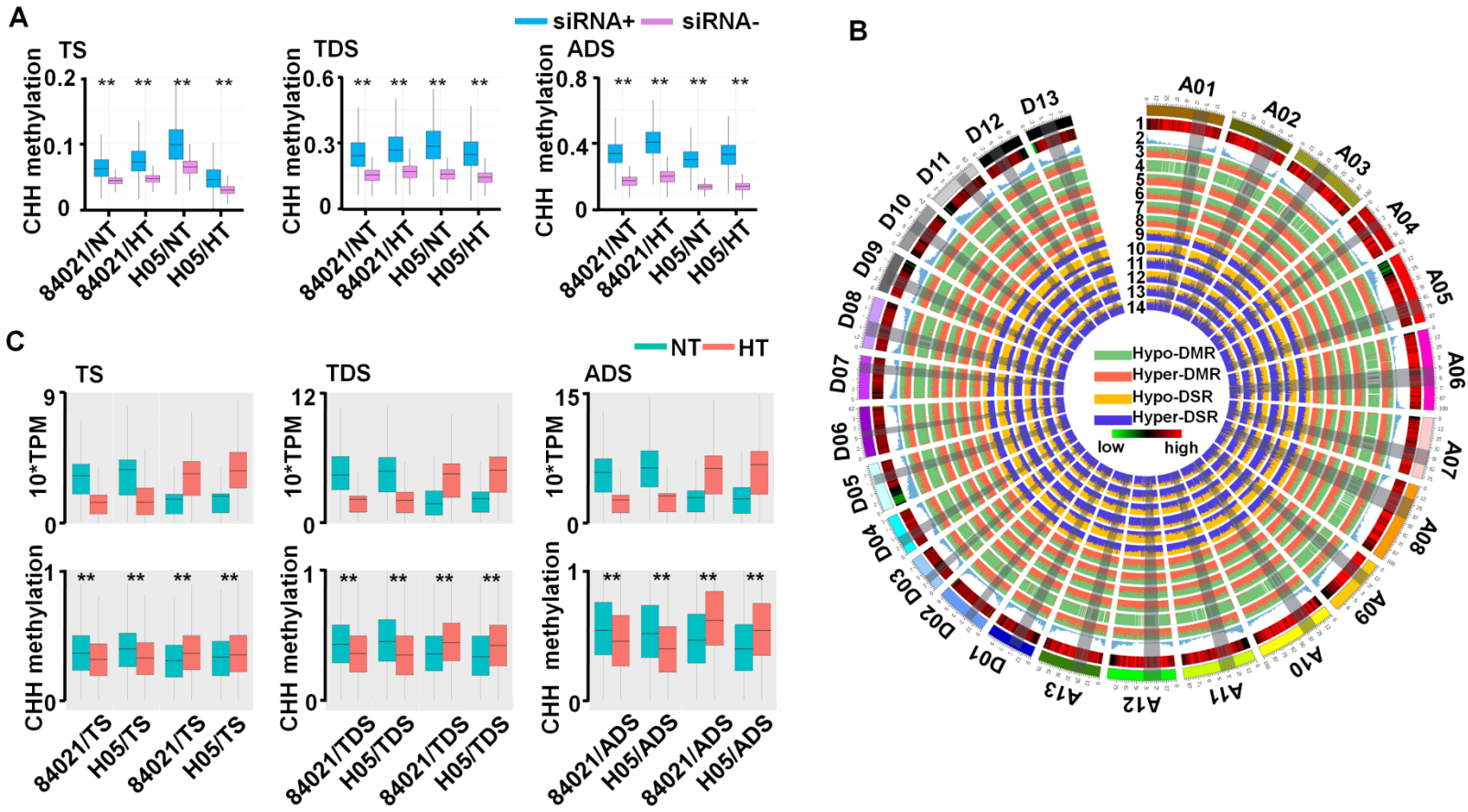

Figure 2. RdDM is involved in regulating CHH methylation under HT.
(A) Identification of CHH methylation in regions containing 24 nt siRNA (siRNA+) and regions lacking 24 nt siRNA (siRNA-) in 1M genomic regions. Hyper-CHH methylation was identified in siRNA+ regions in 84021 and H05 under both NT and HT. Y-axis represents CHH methylation levels. **Significant difference between siRNA+ and siRNA-regions, Student's t-test, $p<0.01$.
(B) Circos plot showing the changes in CHH methylation and 24 nt siRNAs under HT in 84021 and H05 at the tetrad stage (TS), tapetum degradation stage (TDS) and anther dehiscence stage (ADS). The outermost track represents the 26 chromosomes (A01-A13 for the At subgenome and D01-D13 for the Dt subgenome) of the *Gossypium hirsutum* genome. The other tracks represent the following: 1, TE density; 2, number of protein-coding genes (PC genes); 3, CHH differentially methylated regions (DMRs) between 84021/NT/TS (84021 under NT at the tetrad stages) and 84021/HT/TS (84021 under HT at the tetrad stages); 4, CHH DMRs between H05/NT/TS (H05 under NT at the tetrad stage) and H05/HT/TS (H05 under HT at the tetrad stage); 5, CHH DMRs between 84021/NT/TDS (84021 under NT at the tapetum degradation stage) and 84021/HT/TDS (84021 under HT at the tapetum degradation stage); 6, CHH DMRs between H05/NT/TDS (H05 under NT at the tapetum degradation stage) and H05/HT/TDS (H05 under HT at the tapetum degradation stage); 7, CHH DMRs between 84021/NT/ADS (84021 under NT at the anther dehiscence stage) and 84021/HT/ADS (84021 under HT at the anther dehiscence stage); 8, CHH DMRs between H05/NT/ADS (H05 under NT at the anther dehiscence stage) and H05/HT/ADS (H05 under HT at the anther dehiscence stage); 9, differentially siRNA-mapped regions (DSRs) between 84021/NT/TS and 84021/HT/TS; 10, DSRs between H05/NT/TS and H05/HT/TS; 11, DSRs between 84021/NT/TDS and 84021/HT/TDS; 12, DSRs between H05/NT/TDS and H05/HT/TDS; 13, DSRs between 84021/NT/ADS and 84021/HT/ADS; 14, DSRs between H05/NT/ADS and H05/HT/ADS. Data analysis for each chromosome was performed using 1 Mb sections. The approximate centromere regions are indicated by gray boxes. For tracks 3-8, each column represents the ratio between hyper-methylated DMRs and hypo-methylated DMRs, while for tracks 9-14, each column represents the ratio between hyper-DSRs and hypo-DSRs. The ratio between hyper-methylated DMRs and hypo-methylated DMRs is displayed as red columns vs. green columns, and the ratio between hyper-DSRs and hypo-DSRs is presented as purple columns vs. yellow columns.
(C) Identification of CHH methylation levels of differentially siRNA-mapped regions (DSRs) in 84021 and H05 at the tetrad stage (TS), tapetum degradation stage (TDS) and anther dehiscence stage (ADS). Hyper-CHH methylation was identified in the hyper-DSRs, while hypo-CHH methylation was detected in the hypo-DSRs. The Y-axes in the upper panel show siRNA density normalized to 10*TPM, and the Y-axes in the lower panel show CHH methylation levels. The 10*TPM and CHH methylation levels under NT are indicated by blue boxes, and those under HT are indicated by red boxes. **Significant difference, Student's t-test, $p<0.01$.

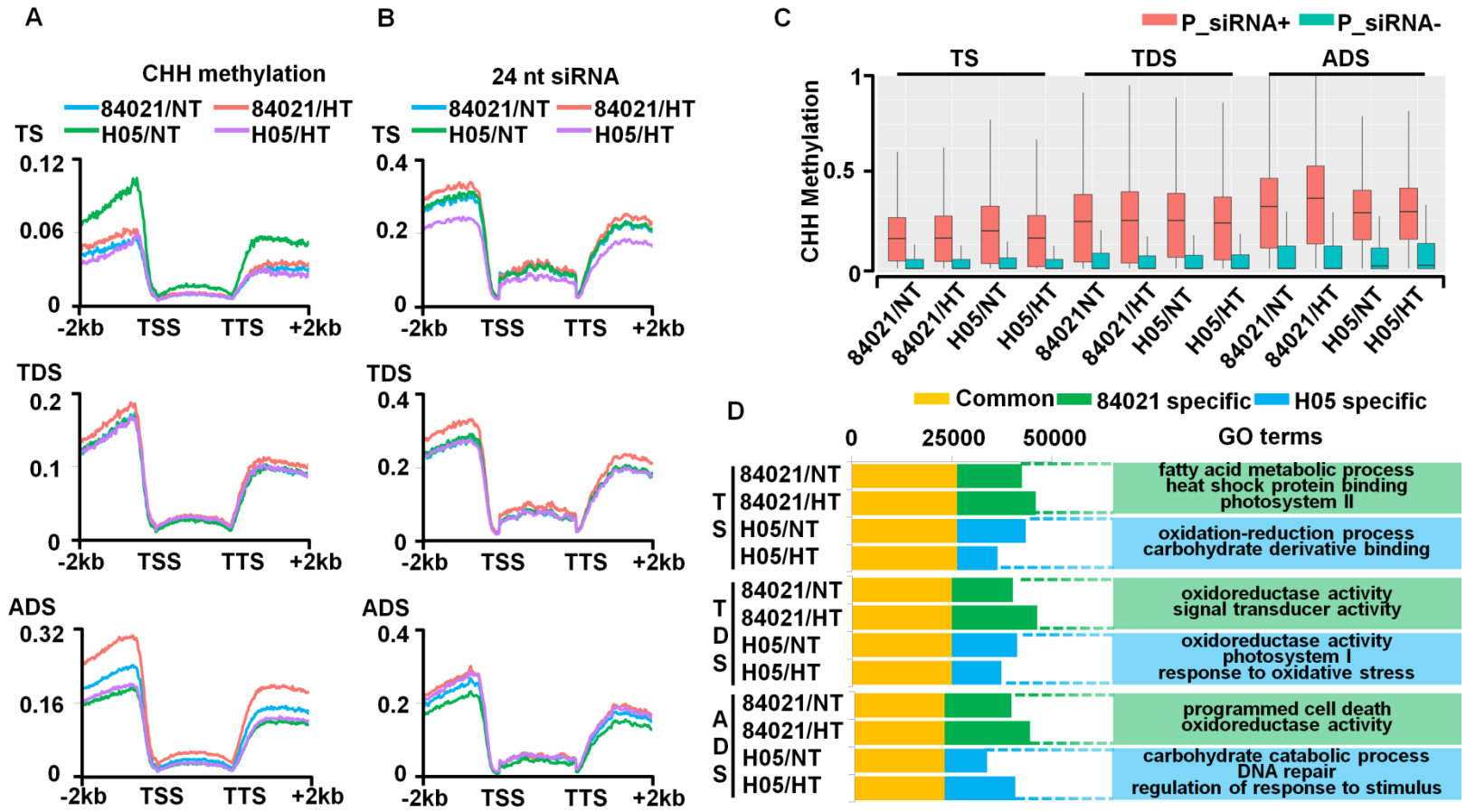

Figure 3. RdDM helps alter CHH methylation in the promoter and downstream regions of protein-coding genes (PC genes).
(A) Analysis of CHH methylation levels in gene regions including promoters (-2kb), gene bodies and downstream regions (+2kb) at the tetrad stage (TS), tapetum degradation stage (TDS) and anther dehiscence stage (ADS) in 84021 under NT (blue lines), H05 under NT (green lines), 84021 under HT (red lines) and H05 under HT (purple lines). Significant differences were detected in the promoter and downstream regions. TSS, Transcription Start Site; TTS, Transcription Termination Site.
(B) Analysis of the density of 24 nt siRNAs in gene regions including promoters, gene bodies and downstream regions in 84021 under NT (blue lines), H05 under NT (green lines), 84021 under HT (red lines) and H05 under HT (purple lines). The density of 24 nt siRNAs also differed in the promoters and downstream regions, as did CHH methylation pattern. TSS, Transcription Start Site; TTS, Transcription Termination Site.
(C) Analysis of CHH methylation of promoters containing 24 nt siRNA sites (P_siRNA+, red boxes) and lacking 24 nt siRNA sites (P_siRNA-, shown in green boxes) in 84021 and H05 at the tetrad stage (TS), tapetum degradation stage (TDS) and anther dehiscence stage (ADS) under NT and HT. The promoters of P_siRNA+ genes showed hyper-CHH methylation compared with those of P_siRNA- genes. There was slight difference in CHH methylation levels among the promoters of P_siRNA- genes.
(D) Number of genes containing 24 nt siRNAs mapped in promoters in anthers at the tetrad stage (TS), tapetum degradation stage (TDS) and anther dehiscence stage (ADS). In anthers at the same developmental stage, genes commonly detected in 84021 under NT, H05 under NT, 84021 under HT and H05 under HT were defined as common genes (yellow columns), and the remaining genes were defined as 84021-specific genes (green columns) and H05-specific genes (blue columns). Enriched Gene Ontology (GO) terms are shown on the right, with cutoff at p-value<0.05.

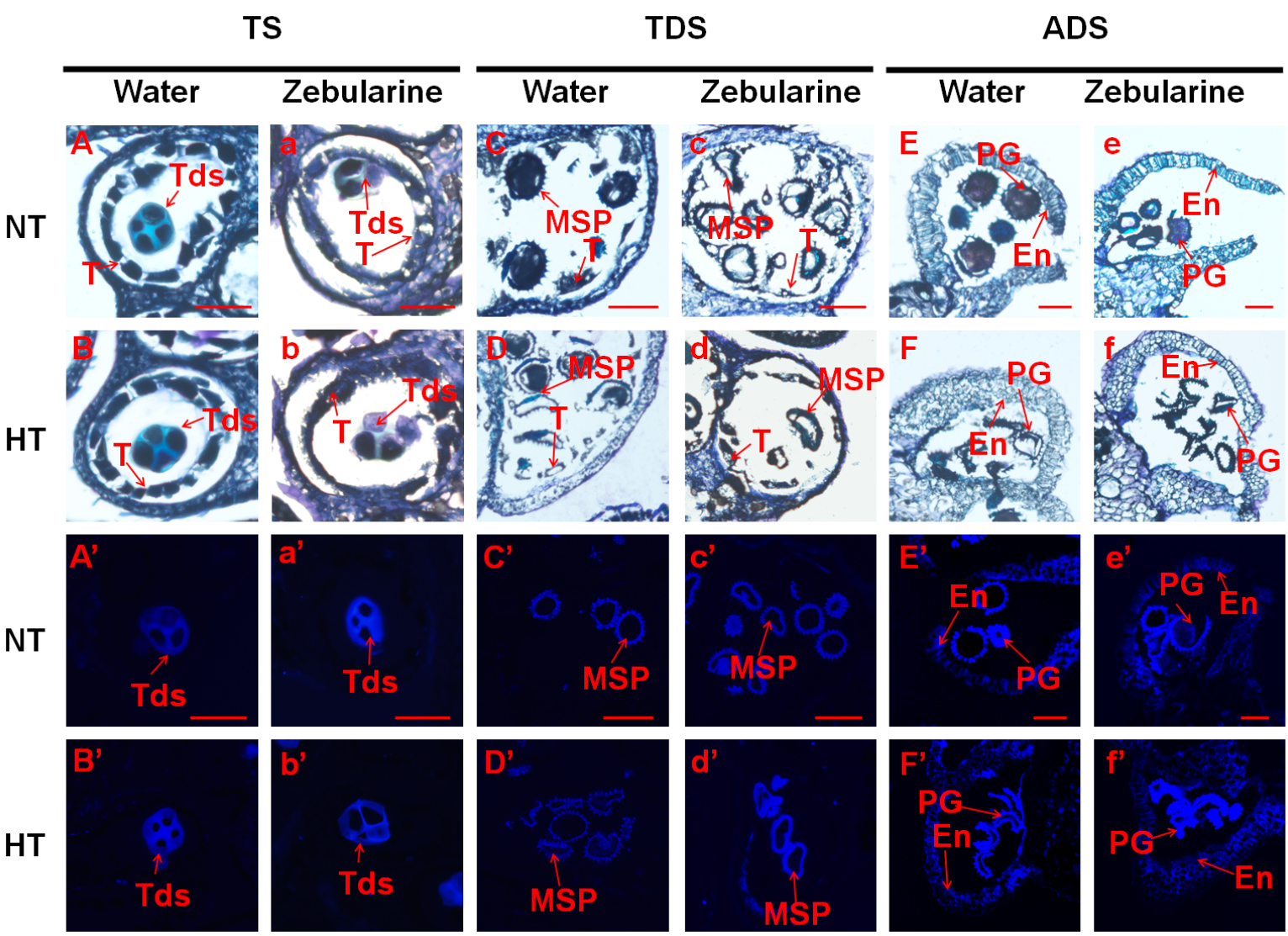

Figure 4. The suppression of DNA methylation induces microspore sterility but does not affect anther dehiscence.
Toluidine Blue staining of anther sections of HNW (H05+NT+Water), HHW (H05+HT+Water), HNZ (H05+NT+Zebularine) and HHZ (H05+HT+Zebularine) at the tetrad stage (TS), tapetum degradation stage (TDS) and anther dehiscence stage (ADS). No obvious changes in tetrads or tapetum were detected under the four treatments at TS **(A)**, **(B)**, **(a)** and **(b)**. At TDS, HT induced abnormal microspore formation in H05 following water treatment **(D)**. H05 showed shrunken microspores following Zebularine treatment under both NT **(c)** and HT **(d)**. At ADS, H05 produced normal pollen only under NT with water treatment **(E).** Dehiscent anther walls and sterile pollen were detected in HNZ **(e)**. Bar=50 μm.
Aniline blue staining of secondary wall thickening was performed under HNW, HHW, HNZ, HHZ treatments at TS, TDS and ADS. No obvious secondary wall thickening was identified at TS and TDS. At ADS, HT induced considerable secondary wall thickening in the endothecium **(F')** and **(f')**, while Zebularine treatment had little effect on secondary wall thickening in H05 under NT **(E'- e')** and HT **(F' - f')**. Bar=50 μm.
Tds, tetrads; T, tapetum; MSP, microspore; PG, pollen grain; En, endothecium

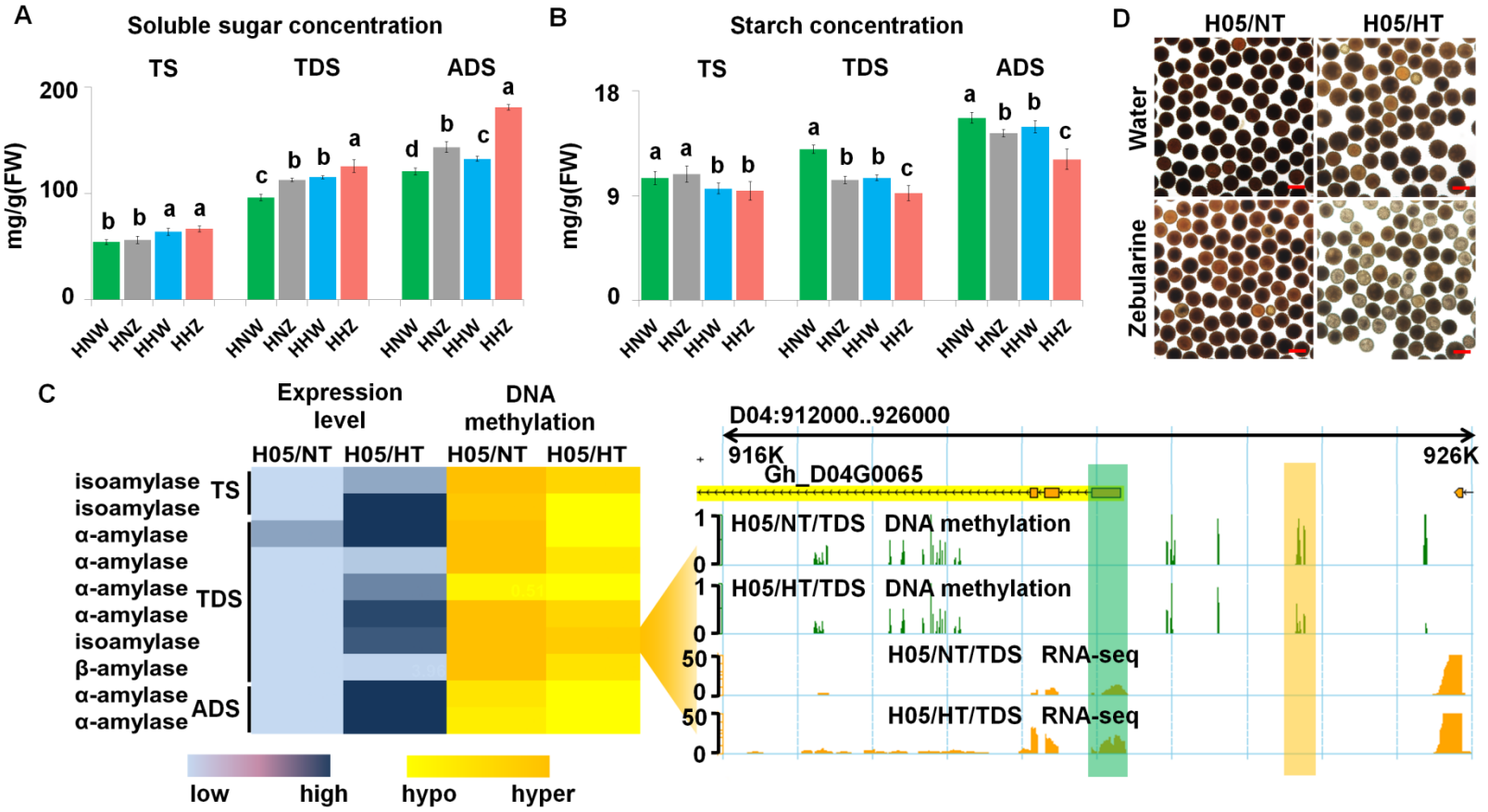

Figure 5. HT-induced DNA methylation is associated with altered sugar metabolism.
(A) Measurement of total soluble sugar contents in HNW (H05+NT+Water), HHW (H05+HT+Water), HNZ (H05+NT+Zebularine) and HHZ (H05+HT+Zebularine) at the tetrad stage (TS), tapetum degradation stage (TDS) and anther dehiscence stage (ADS). Both HT and Zebularine treatment induced sugar accumulation in H05. Values not sharing a common letter are considered significantly different (shortest significant range; $p<0.05$). The values are means ± standard deviation ($n > 5$). FW, fresh weight.
(B) Measurement of starch contents in HNW, HHW, HNZ, HHZ at TS, TDS and ADS. Starch hydrolysis was induced by HT or Zebularine, and increased starch hydrolysis was detected following combined HT and Zebularine treatment. Values not sharing a common letter are considered significantly different (shortest significant range; $p<0.05$). The values are means ± standard deviation ($n > 5$). FW, fresh weight.
(C) The left panel (heatmap) shows the expression levels and DNA methylation levels in the promoters of amylase genes. The right panel (genome browser snapshot) shows DNA methylation levels (orange boxes) in different promoters and different expression levels (green boxes) of an amylase gene at TDS under NT and HT.
(D) I_2-KI staining of starch in pollen of HNW, HHW, HNZ and HHZ. H05 shows considerable starch hydrolysis under HT combined with Zebularine. Bar=50 μm.

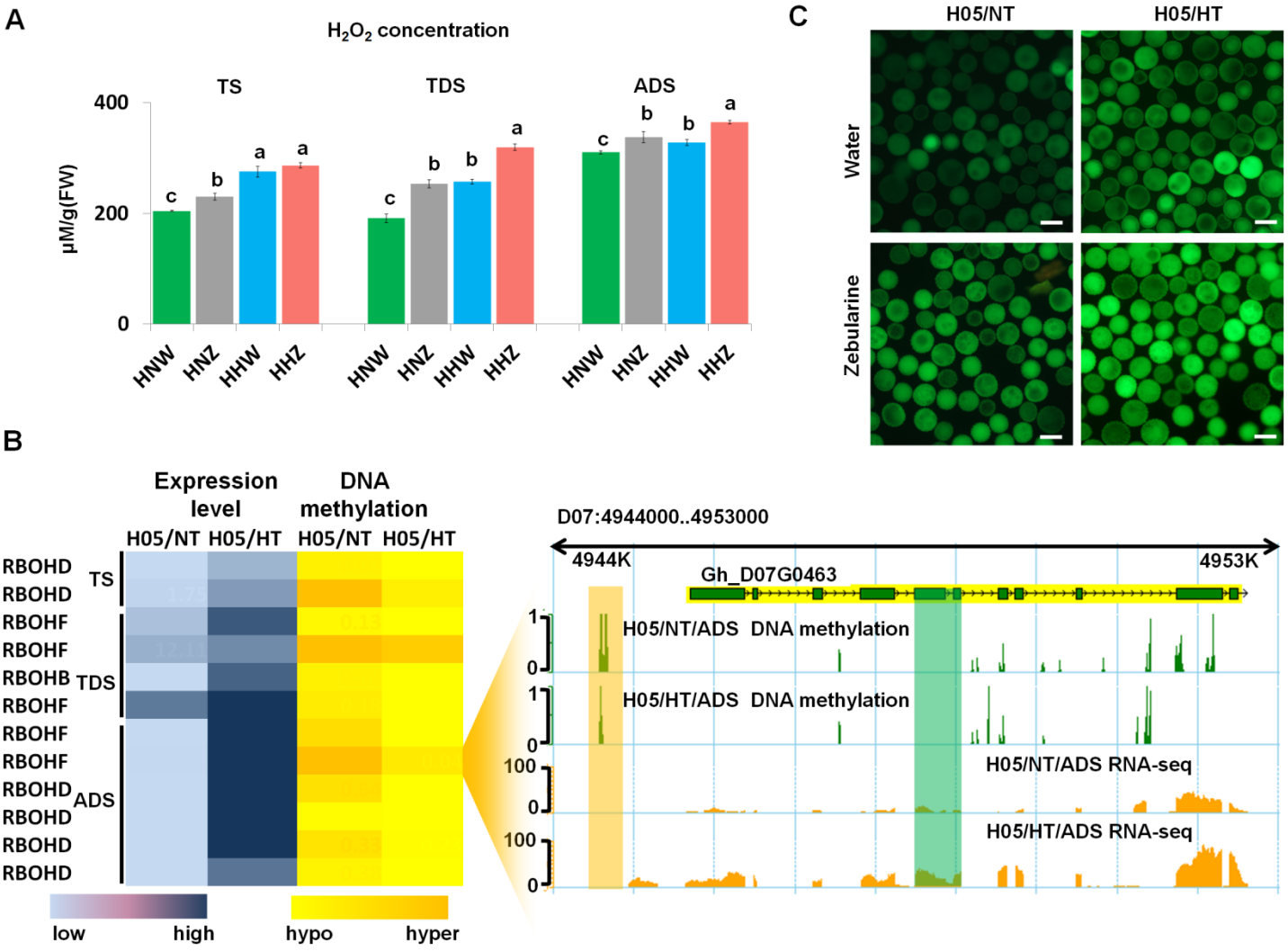

Figure 6. Suppression of DNA methylation induces excessive ROS generation in anthers.
(A) Measurement of H_2O_2 contents in HNW (H05+NT+Water), HHW (H05+HT+Water), HNZ (H05+NT+Zebularine), and HHZ (H05+HT +Zebularine) at the tetrad stage (TS), tapetum degradation stage (TDS) and anther dehiscence stage (ADS). HT or Zebularine induced the generation of H_2O_2, while the combination of HT and Zebularine induced greater accumulation of H_2O_2. Values not sharing a common letter are considered significantly different (shortest significant range; $p<0.05$). The values are means ± standard deviation ($n > 5$).FW, fresh weight.
(B) The left panel (heatmap) shows the expression levels and DNA methylation levels in the promoters of *respiratory burst oxidase homolog* (*RBOH*) genes. The right panel (genome browser snapshot) shows DNA methylation levels in different promoters (orange boxes) and different expression levels (green boxes) of a *RBOH* gene at TDS in H05 under NT and HT.
(C) 2',7'-dichlorodihydrofluorescein diacetate (2',7'-DCFDA) staining of ROS in pollen of HNW, HHW, HNZ, HHZ. HT combined with Zebularine treatment induced increased levels of H_2O_2 accumulation in pollen. Bar=50 μm.

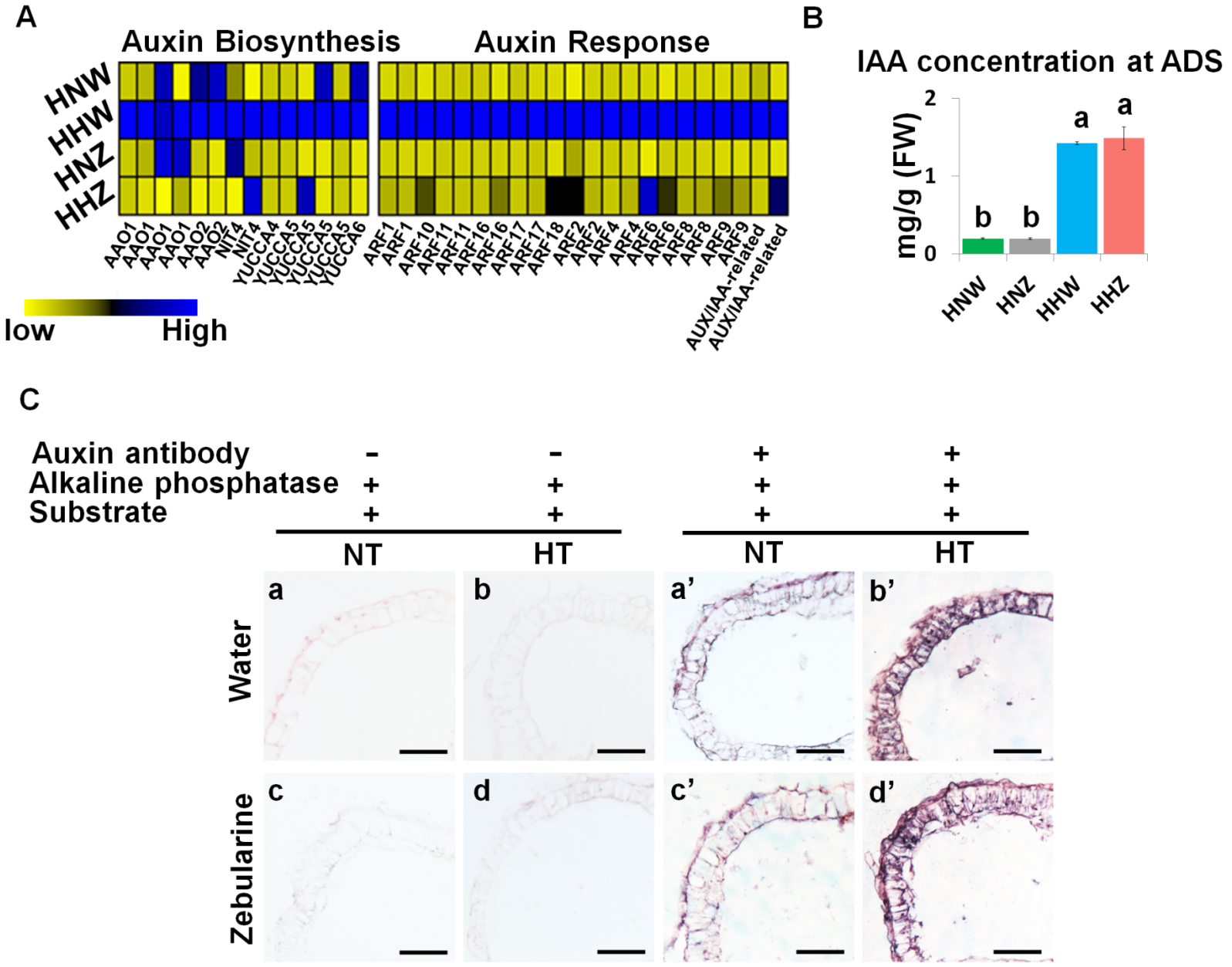

Figure 7. Indehiscence of the endothecium, which is regulated by auxin biosynthesis and signaling pathways, is slightly influenced by HT-disrupted DNA methylation.

(A) A heatmap of the expression levels of auxin biosynthesis and signaling genes at the anther dehiscence stage (ADS) in HNW (H05+NT+Water), HHW (H05+HT+Water), HNZ (H05+NT+Zebularine) and HHZ (H05+HT+Zebularine). Several auxin biosynthesis and signaling genes are up-regulated in HHW, but not induced significantly in HNZ or HHZ. *AAO1*, *ALDEHYDE OXIDASE1*; *NIT4*, *NITRILASE4*; *ARF*, *AUXIN RESPONSE FACTOR*. The genes with the same name (e.g. *AAO1*) represent different copies in the tetraploid cotton genome.

(B) Auxin concentration at ADS in HNW (H05+NT+Water), HHW (H05+HT+Water), HNZ (H05+NT+Zebularine) and HHZ (H05+HT +Zebularine). HT induced significant accumulation of auxin in H05, but the auxin content was not affected by Zeb treatment under either NT or HT. Values not sharing a common letter are considered significantly different. The values are means ± standard deviation ($n > 5$). (Student's t-test, $p<0.05$).

(C) Immunohistochemical assay of auxin in the endothecium in HNW, HHW, HNZ and HHZ. **(a)** to **(d)** show the results of the negative control in HNW **(a)**, HHW **(b)**, HNZ **(c)** and HHZ **(d)** respectively. **(a')** and **(c')** show auxin accumulation in HNW **(a)** and HNZ **(c). (b')** and **(d')** show that HT induces auxin accumulation in the endothecium under HT in response to treatment with water **(b')** and Zebularine **(d')**. Zebularine treatment alters the auxin content only slightly in the endothecium under both NT **(a'** and **c')** and HT **(b'** and **d')**. Bar=50 μm.